In-situ TEM study from the perspective of holders

Toshie Yaguchi[1,*], Mia San Gabriel[2], Ayako Hashimoto[3,4], and Jane Y. Howe[2,5]

[1]Electron Microscope Systems Design Department, Hitachi High-Tech Corporation, 552-53 shinko-cho,Hitachinaka-shi, Ibaraki-ken,312-8504, Japan,
[2]Department of Materials Science and Engineering, University of Toronto, 184 College St, Toronto, ON, Canada.
[3]In-situ Electron Microscopy Technique Development Group, National Institute for Materials Science, 1-2-1 Sengen, Tsukuba 305-0047, Japan.
[4]Degree Programs in Pure and Applied Sciences, University of Tsukuba, 1-2-1 Sengen, Tsukuba 305-0047, Japan.
[5]Department of Chemical Engineering and Applied Chemistry, University of Toronto, 200 College St, Toronto, ON, Canada.

*Correspondence should be addressed to
Toshie Yaguchi[1] , [1]Electron Microscope Systems Design Department, Hitachi High-Tech Corporation, 552-53 shinko-cho,Hitachinaka-shi, Ibaraki-ken,312-8504, Japan
Phone: +81-80-1150-1135
E-mail: toshie.yaguchi.yy@hitachi-hightech.com

Running title: Holders on *in-situ* TEM study

Keywords: *In-situ* transmission electron microscopy, Differential pumping, Closed（sealed）gas cell, Environmental cell, MEM, ETEMS

Total Number of Pages: 72

Number of Figures: 13

Abstract

During the *in-situ* TEM observations, the diverse functionalities of different specimen holders play a crucial role. We hereby provide a comprehensive overview of the main types of holders, associated technologies, and case studies pertaining to the widely employed heating and gas heating methods, from their initial developments to the latest advancement. In addition to the conventional approaches, we also discuss the emergence of holders that incorporate a micro-electro-mechanical system (MEMS) chip for *in-situ* observations. The MEMS technology offers a multitude of functions within a single chip, thereby enhancing the capabilities and versatility of the holders.

MEMS chips have been utilized in the environmental-cell designs, enabling customized fabrication of diverse shapes. This innovation has facilitated their application in conducting *in-situ* observations within gas and liquid environments, particularly in the investigation of catalytic and battery reactions. We summarize recent noteworthy studies conducted using *in-situ* liquid TEM. These studies highlight significant advancements and provide valuable insights into the utilization of MEMS chips in environmental-cells, as well as the expanding capabilities of *in-situ* liquid TEM in various research domains.

Abbreviations

DP: Differential pumping

FLG: few-layer graphene

hBN: hexagonal boron nitride

MEMS: microelectromechanical systems

MoS_2: molybdenum disulfide

SEM: scanning electron microscope(y)

SiN: silicon nitride

STEM: scanning transmission electron microscope(y)

TEM: transmission electron microscope(y)

FIB: focused Ion Beam(system)

UHV: ultra high voltage

E-TEM: Environmental Transmission Electron Microsocpe(y)

HVEM: high-voltage electron microscope(y)

TMP: turbo molecular pump

ED: electron diffraction

SOEC: Solid Oxide Electrolysis Cell

Introduction

In-situ transmission electron microscopy (TEM) is becoming an increasingly useful approach for characterizing materials and their processing. "*In-situ*" is a Latin term that translates to "in its position", and it signifies to capture the real-time process of changing phenomena.

The history of the *in-situ* observation began at the time the electron microscope was invented. In 1935, Marton[1] suggested two methods to restrict or control the gaseous or liquid solutions around specimens. One approach is to build an open environmental chamber with a pair of small apertures that can minimize gas leakage into the column. The apertures maintain the chamber at high pressure while keeping the rest of the column at a low enough pressure. This idea of differential pumping was realized by Ruska [2] and Ardenne [3] respectively, in 1942.

The second approach is to form a closed (sealed) gas cell using electron-transparent windows disposed above and below the sample. The first closed cell with plastic windows was devised by Abrams and McBain [4] from Stanford University in 1944. They observed the movement of liquid and bubbling. The purpose of the initial design was to study the effects of gases on or against contamination by inspecting biological materials in a hydrated state, not *in-situ* observation.

As a means for providing external stimuli to the specimen for *in-situ* observation, there are modified TEM or specially designed specimen holders.

The first reaction specimen chamber compatible with TEM based on differential pumping was developed by Hashimoto et al. [5] in 1968. Using a Pt grid heater with heating capabilities of up to 1000 ºC, the gas pressure of 300 Torr (~4.0 x10^4 Pa) was achieved. In 1971, Swann and Tighe [6] designed a side-entry with single tilt hot stage in portion within the cell gap for the AEI EM7 of a high-voltage electron microscope (HVEM).

In 1962, the solution of the closed cell was demonstrated by Heide [7] [8]. The specimen chamber was formed by two specimen grids and pieces of thin metal foil to determine a constant spacing. The grid was covered with a low contrast film to separate the vacuum pressure of 10^{-6} Torr (1.3x10^{-4} Pa) from the pressure of 760 Torr (1.0x10^5 Pa) in the closed cell. After that, the closed cell was piled up with various improvements (Escaig and Sella, 1966 [9], Fukami, et al. ,1970 [10], Dupouy, 1968 [11]). A closed cell consisted of three films, designed by Fujita et al. [12], held above one atmospheric pressure (1.0 x 10^5 Pa) in 1976.

The idea of *in-situ* liquid TEM proposed in 1935 [1] was inherited by Abrams and Mcbain, who constructed the first enclosed wet cell in 1994 [4]. The cell consisted of two Pt discs, having 0.1 mm holes covered with thin collodion films. An aqueous suspension of the specimen was placed on the lower window. In 1972, Fullam improved this design that had a triple-layer window with an evaporated film of silicon monoxide and the plastic material [13]. Stoyanova et al. (Stoyanova and Mikhailovski, 1959 [14], Stoyanova et al., 1960 [15], 1960 [16]) first investigated the possibility of studying wet biological material in a high-pressure

environmental cell installed in a 75-80 kV microscope. In their design, the environmental cell employed 25 nm-thick collodion/carbon or formvar/carbon composite windows supported across 20–70-μm diameter apertures. The windows were kept apart by a spacer with the thickness ranging from 100 to 2000 μm. For a high-voltage electron microscope (HVEM), a similar cell design was constructed by Dupouy et al. (Dupouy et al.1960 [17]; Dupouy and Perrier 1962 [18]). Allinson designed two side-entry environmental cells in 1970 [19]. The window of single crystal corundum was thinned by ion milling. To avoid the chemical attack of the windows by free water in HVEM, the thick windows of evaporated silicon monoxide deposited on fine mesh copper grids were employed by Nagata and Ishikawa in 1972 [20]. In a side-entry environmental cell reported by Double in 1973 [21], collodion/carbon or collodion/silicon monoxide windows were installed on 200 mesh copper grids. In 1976, Fukami [22] developed a film-sealed environmental cell for a conventional 100 kV TEM. As another observation method for wet specimen, only the lower aperture was served as the film. Using this method, liquid water droplets were observed successfully (e.g., Heide 1962[8]), However, various challenges in the development of liquid environment TEM (ETEM) techniques remain.

The introduction of microelectromechanical systems (MEMS) technology brought a creative advancement in the window approach.

Employing a MEMS-based nano-chip, Creemer et al. [23] miniaturized the gas volume and

heater into a sealed system. Compared to the furnace-based heater, this technique allows a more rapid thermal response and smaller specimen drift. Since then, MEMS has become widely used not only in window approach, but also in aperture approach.

As you can see from the history above, thermal excitation, liquid and/or gaseous environment are examples of typical stimuli used for *in-situ* TEM. These stimuli can be applied directly to the specimen area in a controllable manner by modifications to the microscope, most commonly via specially designed specimen holders.

In this paper. we review the *in-situ* TEM techniques from the perspective of holders having *in-situ* capability of heating and gas/liquid environment.

In-situ **heating TEM**

Here we describe the heating specimen holders for *in-situ* heating TEM technique. There are 2 types of the heating holders. One has an indirect heater and the other is a direct heater.

Furnace-type heating specimen holder

The furnace-type heating holder has a miniature furnace that heats the specimen indirectly. The advantage of this type is that the temperature of the furnace can be measured with a thermocouple. Also, it is designed to use the conventional 3 mm-diameter specimen. The disadvantage of this holder is that the heating region of furnace is rather huge. Because of the size, it takes tens of minutes to achieve a stable target temperature and to eliminate the

specimen drift caused by the thermal expansion. In addition, to operate at a high temperature range, it is often necessary to cool the holder by cooling water.

In 1956, Takahashi et al. developed a furnace-type specimen holder which could heat the specimen up to 1000 ºC [24]. In the next decades, various improvements have been made to reduce the drift by minimizing the heating volume of the heater. In 1986 [25], Sinclair and Parker. developed commercial heating holders and a video-rate recording system which showed mechanical and thermal stability during the heating process. They observed Si re-growth at temperatures between 500 and 800 °C. Heating was implemented with a commercial holder (model number PW 6592), where a Pt pad was heated by an electrical feed-through. The pad held a 3 mm-diameter disk sample, and the temperature was measured using an attached thermocouple. In 2004, M. A. Verheijena et al. [26], modified it for the measurement of the electrical resistance of a TEM sample as a function of temperature.

In 1997, Hidaka et al. [27] developed a double tilt specimen heating holder with a heating element of spiral shaped fine metal wire (Hitachi High-Tech). Direct current is supplied by dry battery to obtain the high-resolution TEM image. The heater is a spiral wire, which is linked to two-stage swirl shape, and then a thin-film bulk sample partially milled by focused ion beam (FIB) is inserted. Using this holder, the transformation from α-Si_3N_4 to β-Si_3N_4 via liquid state was observed during heating. The image of β -Si_3N_4 structure was obtained at 1800 °C with resolution of 0.18 nm. After the modification for the observation of 3

157 mm–diameter disc specimen, the holder has been applied to the study of the oxidation
158 processes of graphene layers on different facets of Pt nanocrystals in Hitachi H-9500 300 kV
159 TEM by Yuan et al. in 2016 [28] [29].
160 In 2019, Shimada et al. [30] have developed an *in-situ* annealing system (Figure 1) that consists
161 of double tilt furnace type heating holder and a new thermal control box with a Proportional-
162 Integral-Differential (PID) controller to improve the spatial and temporal resolution of the *in-*
163 *situ* observations in an aberration-corrected TEM (ARM-200F, JEOL). When the sample was
164 being heated at a rate of +1.0 °C/s, the thermal drift occurred in the parallel to axial holder
165 direction with a rate less than 0.1 nm/s.
166 A widely used double tilt heating holder is Gatan 652 heating holder which employs a Ta
167 furnace with a water-cooling system invented by Jones and Swann [31]. The Ta heater is
168 provided on the outer fringe of the specimen fixed position of about 3 mm-diameter. The thin
169 Ta heater is designed so that the heat responsiveness to the heater current is improved, and it
170 is possible to heat at a maximum of 1273 K (1000 ºC). Although these types of holders
171 improve their stability, a non-ignorable image shift still exists while increasing in temperature.
172 It is not easy to realize the atomic resolution observation especially at temperatures higher
173 than 500 °C, because the recirculating cooling may also bring vibrations and decrease the
174 imaging stability and resolution.
175 Zheng et al. [32] used Themis transmission electron microscope (TFS, 300 kV) with Gatan

652 heating holder for their heating experiments. The growth of C-S-H at various temperatures was investigated. The nanoscale morphology, pore structure, element distribution, and phase transformation were correlated with evaluated temperatures.

Grid-type heating specimen holder/ Wire-type heating specimen holder

In grid-type heating specimen holder or wire-type heating specimen holder, a grid or a fine wire is directly heated by an electric current. Since the specimens are mounted directly onto the heater, they are limited to either powders or flakes. Furthermore, it is hard to directly measure the temperature of the heater. The advantages of this type of holder are the high maximum temperature and high thermal stability.

A simple design of a side-entry single tilt heating holder was built for an HVEM by Swann and Tighe in 1971[6]. The specimen is held between two punched Pt-Rh ribbons 25 μm thick by 3.2 mm wide, which are tensioned by spring-loaded current leads and supported over two quarts fibers 0.5 mm in diameter to minimize heat losses. The spring action absorbs the slack induced by heat expansion. Though the stage is not well insulated, it has a low thermal capacity. Power input is 3 A at 12 V to reach a temperature of 500 ºC, and the maximum operating temperature is 1000 ºC. In 1982, Komatsu et al. [33] developed top-entry stages utilizing localized electron beam heating rather than direct resistance heating of the specimen for ultra-high voltage (UHV) TEM. It consists of a thin Ta tube specimen holder, surrounded by a coaxial Ta tube contains the heater filament and two coaxial stainless

195 steel thermal shields.

196 One example of such a direct type of side-entry single tilt heating holder is Kamino holder or
197 Kamino and Saka holder which was developed by Kamino and Saka [34]. An external view of
198 the Kamino holder is shown in Figure 2. A fine W filament of 25 μm in diameter, which is
199 bridged across two electrodes, is heated by direct electric current from a battery. To obtain
200 thermal stability, a dry battery must be used as a power supply. There are two methods that can
201 be used to calibrate the temperature as a function of the electric current. One method is to use
202 an optical pyrometer outside a TEM. The other is to observe the melting of known materials by
203 *in-situ* TEM. The small thermal mass of the heater leads to a small drift rate. After 15 min., the
204 drift rate becomes as small as 0.1 nm/s. By using the holder, the formation of SiC via solid state
205 reaction between Si and graphite at 1400 °C was successfully observed. On further heating at
206 1500°C, the dynamic observation of a sequence of crystal growth and formation of a grain
207 boundary during sintering at atomic level was achieved [35]. Following this type, two wire
208 types have been developed, which facilitate the heating of more than one material independently
209 [36].

210 Based on this wire type holder, a variety of versions has been developed. For example, a holder
211 consists of the 3 mm-diameter-grid having a support film and 2 W-filaments for sample
212 evaporation as shown in Figure 3 [37]. It was applied to the generation of various composite
213 nanoparticles and the analysis of structural changes at elevated temperatures by Mori et al. in

1994 [38].

As another example, the Kamino holder was modified as a compatible heating holder which can be used in the FIB and the scanning TEM (STEM). Tanigaki et al. demonstrated the *in-situ* heating TEM method for an interface reaction using this holder in 2009 [39]. The specimen was prepared by attaching a micro-sample directly to the heater using the FIB micro-sampling technique (Figure 4). It was confirmed that the EDX map and electron diffraction analyses were possible during the reaction. The resolution of this technique was of the order of 0.223 nm at 550 ^{o}C. The shape of the tip was modified to secure the path of the focused ion beam to the heater while bonding or thinning the micro-sample on the heater. A rotational function was applied to the holder to observe the sample attached to the filament by tilting it 90^{o} from the FIB position. The other modified holders are described in later sections.

In-situ heating TEM – MEMS type specimen holder

The integration of MEMS technology into *in situ* heating TEM specimen holders allows for great customization. MEMS-based heating holders consist of two primary components - a specialized TEM holder and a replaceable chip on which the heating elements are directly patterned. Electrically conductive contact pads on the heating chip directly align with the contact pins on the holder to complete the electrical circuit. MEMS heating chips operate through Joule heating, where a current is driven through the heating element and the electrical energy is converted into heat through resistive losses [40]. The heating element is often

isolated from the bulk of the silicon chip and embedded in a suspended membrane made of SiN or another insulating material. This not only prevents heat transfer to the rest of the chip, but also minimizes sample drift caused by thermal expansion. In some cases, this large membrane is thin enough to double as the electron-transparent region for TEM imaging [41]. However, most recent designs have opted for a thicker SiN membrane patterned with a series of small electron-transparent windows with reduced thickness [42] [43] [44] [45]. The windows are typically circular with diameters ranging from 5-8 μm but vary in size and shape. As the chips serve as both the heating stage and the specimen support, one issue that arises is the bulging of the SiN membrane due to thermal expansion. Van Omme et al. [44] used finite element analysis to simulate the bulging deformations of their heating chip at various temperatures and optimize the design of the Wildfire Heating Nano-chips manufactured by DENSsolutions.

Zhang et al. [46] recently compared the bulging distance, or Z-drift, of the Wildfire chips with the NanoEx heating chips developed by Mele et al. [47]. Both chips exhibited high structural stability at temperatures less than 200° C. However, the NanoEx heating chip was observed to have a significantly larger bulging rate between 200 and 500 °C and a total bulging height of more than 17 μm at 800 °C. Under the same conditions, the Wildfire chip showed minimal bulging behavior until 500 °C and a maximum bulging height of less than 8 μm at 1100 °C.

Over the past several years, many have experimented with different patterns and materials for

optimizing the heating element design. Early heating chips, such as the nanocalorimeter designed by Olson et al. [48] and used by Zhang et al. [41], used a singular, straight heating strip that stretches across a SiN membrane. The Protochips Aduro device used by Allard et al. [49] similarly concentrates the heating region to a small path in a conductive ceramic membrane. In modern heating chips, the heating element is more commonly patterned in a double spiral [42] [43] [44] [45] [50] to optimize Joule heating over the specimen region. Figure 5 shows three examples of the heating element design. Perez Garza et al. [42] designed the double spiral with straight line segments of constant width that follow an octagonal spiral shape, as shown in Figure 5a. In creating the NanoEx heating chips, Mele et al. [47] alternatively patterned a circle in the middle of the heating region surrounded by two heating lines that form hemispheres on either side, shown in Figure 5b. However, these designs introduce corners into the current path, which can result in current crowding [51]. Van Omme et al. [44] designed the DENSsolutions Nano-chips with a double spiral heating element that follows a circular path with no corners to avoid this effect, shown in Figure 5c. While the double spiral design is symmetrical in X and Y directions, it can result in a temperature gradient with the hottest region in the centre of the spiral. Mele et al. [52] proposed that better temperature uniformity can be achieved by increasing the width of the heating element lines closer to the centre of the spiral. This reduced the degree of Joule heating in the central region to counterbalance the nonuniformity of the heating profile. With this configuration, they reported a successful decrease in temperature

variation between the outer and inner regions of the spiral from 15% to 4%. The same concept of increasing linewidth was adopted by van Omme et al. [44] who reported 98% homogeneity over their heating region.

It is common to have at least four contact pads to facilitate four-point probe measurements where current is applied through the two outer contacts, and resistance is measured from the two inner contacts. This allows for resistance measurements without the influence of contact resistance between the contact pins and contact pads [44]. These measurements allow for constant feedback to monitor the temperature of the heating element. Baroncini et al. showed that there is a correlation between the heating power, heating element resistance, and temperature of a microheater that can be quantified using a calibration curve [53].

With MEMS technology, it is possible to increase the functionality of the chip by patterning additional contact pads. Zhao et al. [54] used six contact pads in their heating chip design. Two were used to apply the current to a graphene heating element and four were used to monitor the resistance of a separate platinum thermometer between the heating elements for temperature readings. Bernal et al. [55] reported that the number of contact pads can be increased to at least nine for added functionality in future designs.

Selection of the heating element material is critical in dictating the performance of the heating chip. Several materials have been explored in the development of microhotplates and have since been adopted into heating chip designs. Metallic thin films are advantageous for their

high electrical conductivity, low voltage requirements, and high current density [48]. Platinum is chemically inert at elevated temperatures and has been widely used in MEMS heating devices [47] [50] [56]. Some metals, such as Pt and Ti, require an additional adhesive Cr or Ta layer to be deposited onto the membrane first to avoid delamination [43] [48]. For sensitive applications, this extra layer could influence the electrothermal response and any associated measurements. Mo has been explored as a heating element as it also possesses desirable chemical resistivity, can withstand higher temperatures, and does not require an adhesion layer [42] [43]. However, Mo heating elements require an additional protective layer, such as SiO_2, to prevent oxidation at temperatures over 300 ºC.

Protochips manufactures two types of heating chips – the Fusion Electrothermal E-chips [57] and the Fusion Heating E-chips [58]. The primary difference is that the Fusion Electrothermal E-chips have an additional four tungsten electrodes for electrical characterization of the sample. W has a high melting point of 3422 °C and excellent thermal conductivity, which is compatible with the high temperatures achieved by the heating element [59]. These chips are rated for temperatures up to 900 °C and permit simultaneous heating and electrical measurements. The Protochips designs, unlike the other designs discussed so far, uses a ceramic SiC heating element [58] [60]. Ceramic heating elements have much greater resistance than metal heating elements, and therefore a greater thermal response. Since the resistance of the ceramic heating element is several magnitudes greater than that of the holder-chip contact resistance, the four

point probe setup is not necessary [61]. The Fusion Heating E-chips have only two contact pads and are rated for temperatures up to 1200 °C with temperature accuracy >95 %. DENSsolutions similarly manufactures two sets of chips – the Wildfire Nano-chips for *in situ* heating [62] and the Lightning Nano-chips for *in situ* biasing and heating [63]. The primary difference is that the Lightning Nano-chips have 6-8 contact pads for the additional biasing capability while the Wildfire Nano-chips only have the four contacts required for four-point probe measurements. These chips by DENSsolutions are rated for temperatures up to 1300 °C with temperature accuracy >95 %. In addition to these commercial designs, other materials are still being explored for alternative heating chips. Doped polysilicon has been widely used for heating elements in microheaters outside of ETEM, and shows promising thermal uniformity, stability, and thermal conductivity [53] [64] [65] [66]. However, polysilicon heating elements may encounter issues with long-term stability due to changes in resistivity under thermal and electrical stress [67]. Recently, Zhao et al. [54] used monolayer graphene over suspended SiN as the heating element. They report that the graphene heater has a comparatively low heat capacity, resulting in a fast temperature response, low power consumption, and reduced bulging. On the commercial market, TEM holders for *in situ* MEMS-based heating such as the Protochips Fusion AX holder, DENSolutions Wildfire series, Mel-Build Corporation double tilt 4 electrodes transfer holder, and Hummingbird Scientific MEMS Heating + Biasing holder are available for purchase. Previous studies also list the FEI NanoEx™-i/v single tilt holder [47],

Hitachi Blaze heating holder [68] [69], and Protochips Aduro™ setup [49] as a few additional MEMS type holders. Krisper et al. [70] recently demonstrated the importance of the tilt feature for collecting EDS measurements using the DENSsolutions Wildfire holders. Semiconductor-based EDS detectors, such as silicon-drift detectors, are sensitive to the infrared radiation generated by a heated specimen. Tilt capabilities of the holder can be used to align the EDS detector with low takeoff angles from the sample. At these angles, X-ray signals are collected by the detector, but infrared signals are minimal. Since MEMS-based holders include sidewalls to hold the heating chip in place, low takeoff angles are blocked from the detector and careful optimization of the tilt angle is required.

In-situ **gas heating TEM**

Comparison between opened type and closed type

To produce a controlled atmosphere around the specimen, there are two methods. One is "opened type" or "aperture type". Another is "closed type". Figure 6 shows a schematic diagram of "opened type" specimen chamber(a) and "closed type" one(b).

The "opened type" modifies the specimen chamber by inserting pair of apertures between or within the objective pole pieces to confine the gas leakage, as developed by Boyes and Gai [71]. To avoid a gas leak and maintain the high vacuum in the other critical parts of the TEM, the system would also require the differential pumping system. Therefore, it is also called a

differential pumping type. As there are no additional membranes on windows, it is possible to maintain a high spatial resolution. Unlike closed type E-cells, this type of ETEM system uses the specimen chamber as the reactor and generally does not require specialized holders with gas flow capabilities.

Meanwhile there are some disadvantages of opened type. One major difference is that the opened type system possesses a significantly thicker gas layer than closed type. Currently, the controlled gas pressure in the opened type is lower than in the closed type because the size of the apertures restricts the maximum gas pressure.

In closed type, specially designed TEM holders enclose the specimen between two electron transparent membranes, confining the gas or liquid around the specimen. The important feature of closed type is the airtightness of the cell. The length of gas–electron interaction is much shorter than that in the opened type, making it acceptable to increase the gas pressure. Currently, atomic resolution may be obtained at one atmosphere or higher pressure. Yokozawa et al. reported that their system was evaluated with the (de)hydrogenation of Pd at pressures up to 4.5 bar (4.5×10^5 Pa) [72]. A closed type specimen holder is compatible with different TEMs without any further modifications to the microscope itself. Furthermore, the cost of purchasing or modifying a specimen holder is much smaller compared with an opened type ETEM.

The fracture of the window's membrane or leakage of the gas during experiments would deteriorate the vacuum of the column and electron source. Meanwhile, it is important to ensure

366 the airtightness and field of view during the assembly of the closed cell. This results in the
367 complexity of the specimen loading operation, which involves challenges such as centering the
368 upper and lower window membranes. Furthermore, the electron-transparent window membrane
369 and gas thickness still interact with the electrons, resulting in the scattering information
370 superimposed on the image obtained. Yaguchi et al. reported that the thicknesses of the
371 membranes and the gas channel would have a significant impact on image quality [73]. In
372 addition, the existence of window membranes hindered the acquisition of EDS signals.

373 **Opened type ETEM with heating holders**

374 For *in situ* gas heating experiments, the *in-situ* heating holders can be used in conjunction with
375 the differential pumping ETEM system, also known as the "opened type" ETEM.
376 Hashimoto et al, (1966, 1959) employed a metallic wire with a high melting point as the
377 specimen support while developing [74, 75] the first reaction specimen chamber with apertured
378 environmental TEM. Although high temperature could be achieved by the directly heating the
379 specimen support element, the discharge of gas into the microscope column established a limit
380 of 10 torr (1.3×10^3 Pa). The requirement for differential pumping was then realized to broaden
381 the pressure range of operation. In 1968, Hashimoto et al. [5] modified the specimen stage
382 design and increased the permissible gas pressure to 300 Torr (4.0×10^4 Pa). An electric current
383 was sent through the ribbon to heat the specimen, which was put on a film covering the hole in
384 the Pt ribbon. The gas piped around the object and spilled into the vacuum of the microscope

column via the two Pt holes on either side of the ribbon.

In 1972, Baker and Harris [76] incorporated a modified gas reaction stage (JEOL Co JEM AGI attachment designed by Hashimoto et al. [5,77]) onto a JEM 7A electron microscope. The basic ideas of the ETEM developed by Hashimoto et al. are still used in the latest equipment.

In 1997, Boyes and Gai [71] introduced two pairs of apertures above and below the specimen, which were mounted inside the bores of the objective pole pieces rather than between them as in previous designs so as to keep the high-pressure pathway as small as possible. Additional pumping in the form of turbo molecular and ion getter pumps is used. The gas pressure, usually less than $3x10^3$ Pa, is maintained by a controlled flow directly into the pole piece gap. Thereafter the Titan ETEM G2 was produced by FEI [78] and the more recent Themis ETEM by Thermo Fisher Scientific [79]. The Titan ETEM G2 [78] and Themis ETEM [79] both feature three gas inlets for three different gases, and a mass spectrometer for residual gas analysis of the specimen chamber. All these instruments are additionally configured to support environmental STEM (ESTEM) in addition to ETEM [80].

In 2009, Hitachi H-9500 (LaB_6: 300 kV) *in-situ* TEM featuring with an improved differential pumping capacity for the TEM main unit and mounting a new gas injection mechanism developed by Kishita et al. [81]. There are two vacuum stages developed in the upper portion of the specimen chamber and one vacuum stage in the lower portion, using a turbo molecular pump (TMP) with a pumping speed of 260 L/s. The gaseous atmosphere around the specimen

is created using a nozzle extending from outside of the column to near the specimen. The system configuration permits *in-situ* observation with the specimen temperature of 1200 °C or higher and the pressure in the specimen chamber of ~10 Pa.

In this system, a gas injection port is also provided in the pre-evacuation chamber during the introduction of the specimen holder, which permits heating and gas treatment (equivalent to the atmospheric pressure) in the pre-evacuation chamber. Since the pre-evacuation chamber is a part of the TEM, the specimen can be introduced to the specimen chamber right after the reaction without exposing to air atmosphere. These units allow the observation of unaffected phenomena by the electron beam in processing under the atmospheric pressure. *Ex-situ* observation can be conducted in combination with *in-situ* observation to provide a reliable analysis of structural change processes undergone by various gas treatments.

The Hitachi HF5000 200kV aberration-corrected TEM/STEM employed a combination of small aperture, additional TMP with a pumping speed of 300 L/s, and gas-injection nozzles extending to near the specimen [82] [83] for *in-situ* observation. The Secondary Electron (SE) detector is a key aspect of this system. Lv et al. applied this system with Hitachi High-Tech Canada, Inc. (HTC) MEMS heating holder to verification on oxidation and reduction reactions of perovskite Solid Oxide Electrolysis Cell (SOEC) catalysts for CO_2 electrolysis under gas atmosphere and its CO_2 adsorption sites by E-STEM analysis [84].

Opened type ETEM/Conventional TEM with gas-injection heating holders

In 2005, Kamino et al. [85] developed the side-entry specimen holder consisting of a heating element and a gas injection nozzle. Figure 7 shows an external view of a tip of the holder. It could be attached to a conventional TEM without any modification. The heating element is same as the heating holder as described before. A gas injection nozzle with an inner diameter of 0.5 mm was built about 1mm away from the heating element. This holder provides localized gas atmosphere near the specimen. Therefore, the system enables the user to change the pressure of the specimen chamber in a few minutes.

The experiment was conducted in a Hitachi H-9500 TEM equipped with a LaB_6 cathode. This system allowed for the observation of high-resolution TEM images at temperatures of 1000 ^{o}C in the ~2×10^{-2} Pa gaseous environment in a conventional TEM without any modifications of the vacuum system [81]. Using this TEM, Yaguchi et al. [86] reported the influence of moisture on the structural changes of heated electrocatalysts of polymer electrolyte membrane fuel cells with the combination of the holder and a moisturized air supply system. The morphological changes of a platinum catalyst dispersed on carbon black (Pt/CB) were dynamically observed in the atmosphere of the highly moisturized air. The experimental results at high moisture content were compared with results obtained with lower moisture content. The dependence of morphological changes of the catalyst on the air humidity was clarified.

The holder has been improved to have two built-in heating filaments and an injection nozzle

by Kamino et al. [87] in 2006. Figure 8 shows the design principle and operational workflow of the holder. While one of the heating filaments works as a “Heater”, the other functions as an “Evaporator”. The two heating filaments can be turned on and off independently. When “Evaporator” is turned on, the precursors are evaporated and deposited onto the substrate on the “Heater”. The substrate temperature can be controlled by the “Heater” during and after the evaporation deposition. Gas injection is controlled from outside the TEM column. The entire process, from the synthesis of the Al_2O_3 substrate and deposition of AuPd nanoparticles on the Al_2O_3 support to the observation of nanoparticle behavior on the support surface at elevated temperatures, was done totally *in-situ* within the TEM pole piece gap.

Another modification of the side-entry specimen holder consisting of a heating element is an addition of the air protection transfer mechanism (Figure 9). Using the Hitachi HT7820 TEM (120kV, LaB6) with the holder, the *in-situ* observation of the degradation process was conducted for a sulfide-based Li_4SnS_4 glass ceramic under an air-flow environment by Tsukasaki et al. in 2021[88]. A sulfide-based Li_4SnS_4 glass ceramic is one of the candidates for next-generation all-solid-state batteries materials. Electron diffraction (ED) patterns and hollow cone dark field images could clearly capture morphological changes and the amorphization process caused by air exposure. Moreover, based on the analysis of ED patterns, it is observed that Li_4SnS_4 is likely to decompose because of the reaction with H_2O in air.

Opened type ETEM with MEMS heating holders

For *in situ* gas heating experiments, the MEMS-based *in situ* heating holders previously mentioned in the *In situ heating MEMS type holder* section can be used in conjunction with the differential pumping ETEM system.

These ETEMs have been used with commercial MEMS-based heating holders such as the NanoEx-i/v and DENSsolutions Wildfire holders for a wide variety of *in situ* gas heating applications. While the ETEM/ESTEM systems provide accurate control of gas pressures in the specimen chamber (from 10^{-3} to 2000 Pa for the Themis ETEM), the addition of MEMS technology brings greater control over the temperature of the heating holder and the imaging stability. *In situ* experiments can benefit from greater temperature precision provided by the constant four point probe feedback. Innovative designs of the heating chips also result in a reduction of membrane bulging and thermal drift, which allows for high resolution to be achieved with greater stability. In this section, selected studies that highlight the potential of differentially pumped ETEM with MEMS-based holders are discussed.

In situ studies involving the gas-solid interactions of catalysts is one application which has largely benefited from the advancements in ETEM with MEMS-based holders. The high resolution and stability of the instruments make it possible to image atomic arrangements and investigate the correlation between structure and catalytic performance [89]. These instruments have been particularly useful in the imaging the single-atom interactions involved in catalysis.

When Boyes and Gai first developed their modified ETEM with atomic resolution [90], they reported studies of heterogeneous catalyst reactions. In controlled gas environments of up to 50 mbar (5 kPa), they observed dynamic particle shape changes, growth of passivating sub-nm overlayers, and the transport of C and Ni atoms in the growth process of carbon nanofibers catalyzed by Ni nanocrystals. When they reconfigured the instrument with ESTEM capabilities, they investigated the dynamics of gas-solid catalyst reactions further and achieved atomic resolution of single platinum atoms in 0.02 mbar (20 Pa) H_2 at temperatures greater than 500 °C [80]. The ESTEM addition was highly beneficial for detecting the positions of individual atoms by taking advantage of the HAADF imaging mode with high Z-contrast [91]. However, they reported reduced visibility of single atoms with high mobility at temperatures greater than 400 °C. More recently, Boyes et al. [92] and Martin et al. [93] reported similar single atom dynamic studies, now using the modified JEOL 2200 ETEM/ESTEM with advanced MEMS-based heating holders made by DENSsolutions. Martin et al. studied the migration of single platinum atoms and the evolution of platinum nanoparticle growth in H_2 at temperatures up to 600 °C. Although the resolution is still limited by the high mobility of the loose atoms, they attributed both improved temperature control and stage stability to the MEMS-based holders.

The potential of advanced MEMS-based holders in the imaging of catalytic interfaces was more recently demonstrated by Yuan et al. [94]. They used the DENSsolutions Wildfire S3 heating holder in the FEI Titan 80-300 ETEM to image the real-time epitaxial rotation of Au

nanoparticles on a TiO_2 (001) surface. At 500 °C, they observed a reversible rotational behavior of the nanoparticles when the gas environment in the ETEM was changed. After replacing the oxygen environment [6.5 mbar (650 Pa) O_2] In the chamber with a reactive environment [4.4 mbar (440 Pa) CO/O_2], they concluded that the Au nanoparticle rotated along the [111] axis, perpendicular to the (001) TiO_2 surface. The high stability of the holder was essential to observe the catalyst nanoparticles with atomic resolution under the different environmental conditions. Studies such as these contribute important information about the stability of active catalytic sites and how the catalytic interface can be manipulated through the external environment. Additionally, the phenomenon was found to be temperature dependent as the reversible rotations are not observed at 25 °C. This highlights the benefits of temperature accuracy provided by the MEMS heating chips with four-point probe capabilities. Yuan et al. provide further insights on how these ETEM techniques can be applied in the catalyst design process in their more recent article [95].

These instruments allow for high customizability of the sample environment within the specimen chamber. In addition to common gases such as O_2 or H_2, the ETEM system can accommodate other gaseous species necessary to incite reactions *in situ*. Diallo et al. [60] introduced digermane gas (Ge_2H_6) into the Cs-corrected Titan ETEM to observe the nucleation of Ge crystals on a graphene substrate. They used a Protochips Fusion holder and chip with a SiC ceramic heating element to mount the graphene. Growth temperatures ranged from 220 to

600 °C with and the thermal stability was advertised to be <0.1 °C/min. Studies such as these require slight modifications to the chips themselves. Graphene is electrically conductive and risks short-circuiting the heating elements when mounted onto the heating chip. However, an additional benefit of MEMS-based heating is that the heating chips can easily undergo additional fabrication steps as required. Diallo et al. deposited an extra 10 nm thick Al_2O_3 layer onto the heating chips prior to mounting the electrically conductive graphene sample to electrically isolate them from the heating elements. These sorts of modifications are made possible as the MEMS heating chip devices maintain the flat structure of a standard substrate that is ideal for microfabrication techniques.

Open type E-cell holder with heating

The next system also utilizes the differential pumping effect, that is, “open-type”, but uses a specimen holder or chamber for the formation of the gas phase. In early differential pumping systems, a pair of apertures above and below the specimen were installed into the specimen chamber, and the apertures could be taken in/out from the microscope vacuum through the airlock along with the specimen chamber [5,76,77,96].

On the other hand, when a differential pumping unit is attached to a side-entry specimen holder, as an open-type cell, a conventional TEM can be used without any modification to the TEM column because the holder is independent of the TEM main body. However, as the tip of the specimen holder is inserted into the gap between the pole piece of objective lens, there are

significant size restrictions. Since the differential pumping mechanism must be built into the thickness of a few mm, multiple orifice pairs can be hardly arranged unlike an ETEM, and consequently atmospheric pressure cannot be reached. In other words, observations at a lower gas pressure, for example, in the case of a catalytic reaction, will result in fewer gas molecules as the reacting species, thereby reducing the reaction rate. Therefore, it is easier to capture the behavior during the reaction even with a standard CCD camera.

Hashimoto et al. developed and used such differential pumping specimen holder system for the *in situ* observation of catalytic materials [97]. Figure 10 shows a side-entry specimen holder with differential pumping unit and MEMS heating device, which does not use single orifice pair. As shown in Figure 10 (a) the system consists of a differential pumping unit and a MEMS heating unit. The gas reaching near the specimen through a nozzle leaks out through the paired orifices to the vacuum of the microscope column. As a consequence, it is difficult to use corrosive or wetting gases. The inner pressure can be kept up to 20 Pa higher than that of the outer column. For the reduction of microscope vibration, the specimen holder grip (Figure 10 (b)) contains a gas tank in order to be used without the connection with an exterior gas source during observation, and the fine control valves driven by a piezo actuator in order to control gas flow electrically. The inner pressure near the specimen can be measured by a tiny pressure gauge. For specimen heating, the specimen is placed on a MEMS heater with holes, which also serves as an orifice as shown in Figure 10 (c) and (d). Shoji el al. observed the Ni#Y_2O_3 catalyst

556 with entangled networks of tens-of-nanometer-thick fibrous phases as catalytic materials for
557 CH_4 conversion (Figure11) [98]. Their *in-situ* TEM/STEM imaging and EELS analysis showed
558 that the Ni center of the Ni#Y_2O_3 region was stable for its structure and valence state because
559 of its topologically immobilized structure (Figure 11 (b) and (c)), which would contribute to its
560 long-term stable catalytic performance.
561 Next, instead of using a side-entry specimen holder, a differential-pumping-type chamber (cell)
562 that can be inserted and removed in the HVEM. HVEMs have been used for not only
563 observation of thick biological samples, polymers, metals etc. but also improvement of the
564 point-to-point resolution. As a technique to improve such resolution, the use of spherical
565 aberration correctors has been developed and then has been reported for various applications.
566 However, HVEMs are still necessary for observation of thick specimens, and has the feature of
567 the wider gap between the pole pieces of the objective lens, which should be advantageous to
568 *in-situ* observations.
569 As shown in Figure 12(a), Tanaka et al. [99] developed an environmental HVEM (E-HVEM)
570 with using a differential-pumping-type cell, named 'Reaction Science HVEM' (JEOL;
571 JEM1000 K RS), whose high-voltage tank housing as accelerating tube is 6.7 m in height and
572 column is 3.6 m in length. This E-HVEM utilized a symmetrical objective lens with a polepiece
573 gap larger than 15 mm for formation of gas phase, where a new side-entry goniometer to enable
574 inserting and retracting the gas chamber as the environmental open-type cell was constructed

575 as shown in Figure 12 (b) [100]. For adopting the open E-cell, three-stage differential pumping
576 system was installed into around the objective lens with additional five turbo molecular pumps
577 and a scrolled pump. This open type E-cell produced a few tenth of atmosphere, for example,
578 13,300 Pa (=100 Torr), which is larger than typical ETEM. Standard various specimen holders
579 including heating ones can be inserted into the gas chamber for various *in-situ* observation. A
580 point-to-point resolution in TEM and STEM mode was less than 0.15 nm and 1 nm at an
581 accelerating voltage of 1 MV, respectively. Furthermore, a quadrupole mass spectrometer
582 (QMS) was combined to identify the reaction gases *in-situ* in the specimen chamber [101].
583 Fujita et al. [102] observed nanoporous NiCo catalyst used also for CH_4 conversion through E-
584 HVEM in order to investigate the origin of the moderate activity and thermal stability. The
585 grains in the ligaments became finer when the mixture gas (CH_4 + CO_2) was introduced into
586 the specimen chamber heating at 600 ºC, although the pore/ligaments coarsened during heating
587 at 600 ºC in vacuum. Furthermore, STEM-EDS analysis of the cooled sample showed the
588 chemical demixing of Ni and Co. This grain refinement and chemical demixing can imply
589 "synergic effects", which demonstrated higher catalytic activity and durability of bimetallic Ni–
590 Co.
591 Closed-type E-cells with membranes, which are generally used in the specimen holder, are
592 necessary for observation in gas atmospheres above atmospheric pressure or in liquids. In
593 addition, any modifications of TEM are not required.

However, the membranes and dense gas phases sometimes deteriorate image resolution. Furthermore, they become a background and reduce the accuracy when combined with analysis methods such as EELS and holography. In contrast, although the open-type specimen holder or chamber produce the lower ultimate pressure than close-type E-cells, this system has the potential to achieve higher image resolution and less background for EELS analysis and holography than not only the close-type E-cells but also the typical modern ETEM with the larger thickness of the gas phase.

Closed type ETEM/E-cell heating holders

As mentioned in the previous sections, there are mainly two approaches that enable TEM study of materials in gaseous atmosphere. One is to directly introduce gas to the sample vicinity while maintaining high vacuum elsewhere through the pressure-limiting differential pumping (DP) system. Boyes and Gai developed such system in the 1990's, modifying a Philips CM30 TEM, achieving an impressive 0.2 nm resolution and 50 mbar (5 kPa) [71]. Later, they built the similar system on aberration-corrected TEM [90]. The advantage of this approach is permitting the use of regular sample holder or windowless heating holder. Spatial resolution is higher because its windowless configuration. However, this approach limits the highest gas or vapor pressure to ~ 100 mbar (10 kPa). Another approach is to introduce gas through closed window cell as part of the sample holder. Such environmental cell, called "E-cell" in this paper, is a type of MEMS-based devices with electronically transparent windows typically made of amorphous silicon nitride (SiN_x). Closed E-cell has the advantage of

accommodating high gas or vapor pressure. Gas pressure up to 4 bar (400 Pa) has been achieved [103]. Unlike the open system, which requires customized design and build of an *in-situ* electron microscope, by having the E-cell sample holder on any matching microscope, it can readily perform TEM analysis in gas. If the E-cell has a hermetic seal, it can also hold liquid or liquid and gas/vapor mixture, which is reviewed in next section.

An example of E-cell by Protochips [104] is presented in Figure 13. Dai et al.[105] studied the Rh-doped $CaTiO_3$ powder near atmospheric pressure ranged from 250 to 700 ^oC using aberration-corrected scanning transmission electron microscopy. It revealed both cyclical precipitation−dissolution of Rh nanoparticles in response to redox cycling of the ambient gas and sintering of the powder [105].

In-situ liquid-phase electron microscopy

Liquid cell electron microscopy is an emerging technique that allows *in situ* imaging and control of nanoscale phenomena in hermetically sealed liquid cell using TEM, STEM or SEM [106, 107]. To be compatible with the vacuum environment required by the TEM, most of the liquid-phase microscopy studies have been carried out using sealed cells. The first report of closed-cell design was proposed by Abrams and McBain in 1944 [108]. MEMS-based liquid-cell is the enabling technology which drives the liquid-phase microscopy study over the past two decades. In 2003, Ross et al first reported using the silicon nitride E-cell to study nucleation and growth

633 of copper clusters in aqueous solutions [109]. This liquid cell has a liquid reservoir and two
634 electrodes. TEM study was carried out using a Hitachi H-9000 TEM operated at 300 kV right
635 after the E cell was connected to a power source for observing the Galvanic growths. Images
636 and videos were recorded during galvanostatic deposition with cathodic current densities of 5
637 and 50 $mAcm^{-2}$. In 2009, Zheng et al. [110] studied the colloidal nanocrystal growth using a
638 JEOL 3010 TEM. It shows that the platinum nanocrystals can either grow by monomer
639 attachment or by particle coalescence. These two type cells were static cell, which had no liquid
640 flow. Liquid flow cells have become commercially available through various vendors. Liquid
641 flow cell with electrical leads or built-in electrodes permits electrochemical analysis of
642 materials *in situ.* There are also designs to incorporate a thin-film Joule heater, allowing heating
643 the liquid to its boiling point. Hummingbird has recently developed an optical liquid
644 electrochemistry holder, which makes possible to study photocatalysis, photoelectrochemistry
645 or photochemistry [111].
646 It is also possible to map the electrostatic potentials and magnetic fields in liquids using off-
647 axis electron holography [112]. Prozorov et al. demonstrated that the Magnetospirillum
648 magneticum strain AMB-1 and assemblies of magnetic nanoparticles can be studied using off-
649 axis electron holography. The electron holograms show sufficient interference fringe contrast
650 to allow the reconstruction of the phase shift of the electron wave and mapping of the magnetic
651 induction from bacterial magnetite nanocrystals.

652 Most of commercially available liquid cells have amorphous silicon nitride (SiN) windows for
653 observation. The SiN window can hardly be thinner than 8 nm. SiN is also a dielectric material
654 with a bandgap of 5 eV. It is considered as an electrical insulator, which has charging problem.
655 Ideally, the window membrane should be electronically transparent, mechanically robust,
656 chemically inert, with good electronical and heat conductivity. Low atomic number 2D
657 materials such as hexagonal boron nitride (hBN) and graphene have been experimented for
658 making liquid cells with some success. Initial designs of graphene liquid cell rely on pockets of
659 liquid randomly stored in between two graphene sheets [113].
660 Clark et al. fabricated liquid cells using lithographically patterned few-layer graphene (FLG),
661 molybdenum disulfide (MoS_2), and hBN membranes [114]. Illustrated in Figure 14, it has a
662 monolayer of MoS_2 sealed between FLG, with hBN as spacers. They reported that atomically
663 flat hBN sheets form a hermetic seal with graphene and MoS_2. This design has a highly
664 controlled total thickness of less than 70 nm which enables single atom tracking. This method
665 could be applicable to a wide variety of applications in not only physical sciences but other
666 fields of research.
667
668 **Concluding remarks and Outlook**
669 We have reviewed the *in-situ* TEM techniques, focusing on holders for high temperature, gas
670 reaction, and liquid environments. Those techniques enable the real-time observation of

materials responses at the atomic scale under specific conditions.

In the context of *in-situ* heating TEM, aside from powder and the 3 mm-diameter disc specimens, it is also feasible to handle specimens prepared using FIB processing. By combing these holders with E-TEM, the *in-situ* gas heating experiments can be carried out. The E-cell holders utilizing MEMS technology are capable of precise temperature control during the *in-situ* liquid and gas heating experiments. These E-cell holders, along with gas-injection holders, can be utilized in TEM with standard setups. Choosing the appropriate holder aligned with specific experimental goals greatly facilitates *in-situ* TEM studies.

A major challenge in general *in-situ* research is efficient quantitative data acquisition. This can be addressed through the design of simplified and repeatable workflows, as well as through AI-assisted data acquisition and data interpretation. Additionally, there is a need for a deeper understanding of the interaction between the electron beam and the specimen. Controlling the dose of electron beam is crucial to minimize radiolysis effects. Another approach is to improve the temporal resolution of in-situ TEM by using pulsed electron source [115, 116].

In the case of liquid-phase microscopy, advancements in liquid cell design are necessary to address two key aspects: 1) controlling the flow and Brownian motion; and 2) better control over the liquid thickness. By addressing these challenges, *in-situ* TEM offers unprecedented opportunities to elucidate of material functionality and dynamics with atomic-level precision and high temporal resolution across various fields.

Acknowledgements

MSG thanks the support by the Ontario Graduate Scholarship. JYH ack acknowledges the support by the Natural Sciences and Engineering Research Council (NSERC) of Canada._

AH thanks the financial supports by Precursory Research for Embryonic Science and Technology (PRESTO) [No. JPMJPR17S7], Japan Science and Technology Agency (JST), and Grant-in-Aid for Scientific Research (C) (KAKENHI) [No. 25390035], Japan Society for the Promotion of Science (JSPS).

Data Availability Statements

No new data were generated or analysed in support of this research.

Conflict of Interest

The authors declare that they have no conflict of interest.

References

[1] Marton L (1935) La microscopie electronique des objets biologiques. *Bull. Sci Acad R Belg*. 21: 553.

[2] Ruska E (1942) Beitrag zur übermikroskopischen Abbildung bei höheren Drucken. *Kolloid-Zeitschrift.* 100(2):212-219.

[3] von Ardenne M (1942) *Reaction chamber* supermicroscopy by means of the universal electron microscope. *Z. physik. Chem.* B 52: 61-71.

[4] Abrams I M and McBain J W (1944) A closed cell for electron microscopy. *J Appl Phys.* 15(8): 607-609.

[5] Hashimoto H, Naiki T, Eto T, and Fujiwara K (1968) High temperature gas reaction specimen chamber for an electron microscope. *Jpn J Appl Phys.* 7(8): 946-952.

[6] Swann P and Tighe N (1971) High voltage microscopy of gas oxide reactions. *Jernkontorets Annaler.* 155(8): 497-501.

[7] Heide H G (1960) Elektronenmikroskopie von Objekten unter Atmosphärendruck oder unter Drucken, welche ihre Austrocknung verhindern. *Naturwissenschaften.* 47(14): 313-317.

[8] Heide H G (1962) Electron microscopic observation of specimens under controlled gas pressure. *J Cell Biol* 13(1): 147-152.

[9] Escaig J and Sella C J. Escaig and C. Sella,(1966) Object cell for observing specimen heated under controlled atmosphere. *Proc. 6th Int,Congress for Electron Microscopy.* 1: 177.

[10] *Fukami A, Etoh T,* Ishihara N, Katoh M, and Fujiwara K (1970) Pressurized specimen chamber for electron microscope. *Proc. 7th Int. Congress on Electron Microscopy*. 1: 171.

[11] Dupouy G (1968) Electron Microscopy at Very High Voltages, In: Barer R and Cosslett V E (ed.) *Adv. Opt. Electron Microsc. 2: pp.168-250 (*Academic Press).

[12] Fujita H, Komatsu M, and Ishikawa I (1976) A universal environmental cell for a 3MVclass electron microscope and its applications to metallurgical subjects. *Jpn J Appl Phys.* 15(11): 2221-2228.

[13] *Fullam E F (1972)* A *Closed* wet cell for electron-microscope. *Rev. Sci. Instrum.* 43: 245-247.

[14] *Stoyanova* I G and *Mikhailovski* G A (1959) Method and apparatus for studying wet objects in the electron microscope. *Biophysics.* 4: 116-121.

[15] Stoyanova I G, Nekrasova T A, and Zaides A L (1960) A study of collagen in humid condition in a gas microchamber of an electron microscope. The effect of Ionizing Radiation on collagen. *Doklady Akad. Nauk S.S.S.R* 130：1366-1369.

[16] Stoyanova I G, Nekrasova T A, and Biryuzova V I (1960) Study of action of radiation on bacterial cells in moist microchamber of electron microscope. *Doklady. Biological Sciences.* 131(1-6): 185-188.

[17] Dupouy G, Perrier F, and Durrieu L (1960) Observation of living matter by means of a high voltage electron microscope. *C. r. hebd. Séanc. Acad. Sci., Paris.* 251: 2836-2841.

[18] Dupouy G and Perrier F (1962) Microscopie electronique fonctionnant sous une tension

759 d'un million de volts. *J. de Microscopie.* 1: 67-92.
760
761 [19] Allinson D L (1970) Environmental cell for use in a high voltage electron microscope. *7th*
762 *Int. Congr. Electron Microscopy. Grenoble.* I: 169-170.
763
764 [20] Nagata F and Ishikawa I (1972) Observation of wet biological materials in a high voltage
765 electron microscope. *J. Appli. Phys.* 11: 1239-1244.
766
767 [21] Double D D (1973) Some studies of the hydration of portland cement using high voltage
768 (1MV) electron microscopy. *Mat. Sci. Eng.* 12: 29-34.
769
770 [22] Fukami A (1974) Merit and Demerit of Observation Method Using Environmental Cell. *J*
771 *Electron Microsc.* 23(1): 64.
772
773 [23] Creemer F, Helveg S, Hoveling G H, Ullmann S, Molenbroek A M, Sarro P M, and
774 Zandbergen H W (2008) Atomic-scale electron microscopy at ambient pressure.
775 *Ultramicroscopy.* 108: 993-998.
776
777 [24] Takahashi N, Takeyama T, Ito K, Ito T, Mihama K, and Watanabe M (1956) High
778 temperature furnace for the electron microscope. *J Electron Microsc.* 4(1): 16-23.
779
780 [25] Sinclair R and Parker MA (1986) High-resolution transmission electron microscopy of
781 silicon re-growth at controlled elevated temperatures. *Nature.* 322(6079): 531-533.
782

[26] Verheijena M A and Donkers J J T M, Thomassen J F P, van den Broek J J , van der Rijt R A F, Dona M J J, and Smit C M (2004) Transmission electron microscopy specimen holder for simultaneous *in situ* heating and electrical resistance measurements. *Rev. Sci. Instrum.* 75(2): 426-429.

[27] Hidaka K, Fujiwara T, and Kamino T (1997) Trial Manufacturing of Heating Stage for *In-situ* Observation by TEM. *Journal of Surface Analysis.* 3(2): 431-434.

[28] Yuan W, Wang Y, Li H, Wu H, Zhang Z, Selloni A, and Sun C (2016) Real-Time Observation of Reconstruction Dynamics on TiO_2(001) Surface under Oxygen via an Environmental Transmission Electron Microscope. *Nano Lett.* 16: 132-137.

[29] Yuan W, Jiang Y, Wang Y, Kattel S, Chou L Y, Tsung C K, Wei X, Li J, Zhang X, Wang G, Mao S X, and Zhang Z (2015) *In situ* observation of facet-dependent oxidation of graphene on platinum in an environmental TEM. *Chem. Commun*. 51: 350-353.

[30] Shimada Y, Yoshida K, Inoue K, Shiraishi T, Kiguchi T, Nagai Y, and Konno T J (2019) Evaluation of spatial and temporal resolution on *in situ* annealing aberration-corrected transmission electron microscopy with proportional–integral–differential controller. *Microscopy*. 68(3): 271–278.

[31] Jones J S and Swann P R (1991) Specimen heating holder for electron microscopes. *United States Patent,* No. 4,996,433.

[32] Zheng Q, Jiang J, Xu G, Yu J, Tang L, and Li S (2020) New insights into the role of

Portlandite in the cement system: elastic anisotropy, thermal stability, and structural compatibility with CSH. *Cryst, Growth Des.* 20: 2477-2488.

[33] Komatsu M, Fujita H and Matsui H (1982) A new type of very-high temperature heating stage and *in situ* experiments on α-Al_2O_3 crystals. *Jpn. J. Appl. Phys.* 21 (8) : 1233-1237.

[34] Kamino T and Saka H (1993) Newly developed high resolution hot stage and its applications to materials science. *Microsc. Microanal. Microstruct.* 4: 127-135.

[35] Kamino T, Yaguchi T and Saka H (1994) *In Situ* Study of Chemical Reaction between Silicon and Graphite at l,400°C in a High Resolution/Analytical Electron Microscope. *J Electron Microsc.*. 43(2): 104-110.

[36] Kamino T, Sasaki K, and Saka H (1997) High Resolution Electron Microscopy In Situ Observation of Dynamic Behavior of Grain Boundaries and Interfaces at Very High Temperatures. *Microscopy and Microanalysis.* ***3***(5): 393-408.

[37] Yasuda H (1997) Spontaneous alloying in nanometer-sized particles. *Denshikenbikyou*. 32(1): 17-22 (in Japanese).

[38] Mori H, Yasuda H, and Kamino T (1994) High-resolution electron microscopy study of spontaneous alloying in gold clusters. *Philosophical magazine letters.* 69(5): 279-283.

[39] Tanigaki T T, Ito K, Nagakubo Y, Asakawa T, and Kanemura T (2009) An *in situ* heating TEM analysis method for an interface reaction. *J Electron Microsc.* 58(5): 281-287.

[40] Geisberger A A and Sarkar N (2006) Techniques in MEMS Microthermal Actuators and Their Applications. In: Leondes C T (ed.) *MEMS/NEMS*. pp. 201-261, (Springer, Boston).

[41] Zhang M, Olson E A, Twesten R D, Wen J G, Allen L H, Robertson I M, and Petrov I (2005) In situ transmission electron microscopy studies enabled by microelectromechanical system technology. *J. Mater. Res.* 20(7): 1802-1807.

[42] Perez Garza H H, Morsink D, Xu J, Sholkina M, Pivak Y, Pen M, van Weperen S, and Xu Q (2016) MEMS-based nanoreactor for in situ analysis of solid-gas interactions inside the transmission electron microscope. *Micro Nano Lett.* 12(2): 69-75.

[43] Mele L, Santagata F, Mihailovic M, Rossi T, Tran A T, Schellevis H, Creemer J F, and Sarro P M (2012) A molybdenum MEMS microhotplate for high-temperature operation. *Sens. Actuator A Phys.* 188: 173-180.

[44] van Omme J T, Zakhozehva M, Spruit R G, Sholkina M, and Perez Garza H H (2018) Advanced microheater for in situ transmission electron microscopy; enabling unexplored analytical studies and extreme spatial stability. *Ultramicroscopy* 192: 14-20.

[45] Norcada Inc., "MEMS IN-SITU HEATING," [Online]. Available: https://www.norcada.com/products/in-situ-tem/. [Accessed 15 May 2023].

[46] Zhang F, Zhang X, Jia Z, and Liu W (2022) Precise drift tracking for in situ transmission electron microscopy via a thon-ring based sample position measurement. *Microsc. Microanal.* 28: 1945-1951.

[47] Mele L, Konings S, Dona P, Evertz F, Mitterbauer C, Faber P, Schampers R, and Jinschek J R (2016) A MEMS-based heating holder for the direct imaging of simultaneous in-situ heating and biasing experiments in scanning/transmission electron microscopes. *Microsc. Res. Tech.* 79: 239-250.

[48] Olson E A, Efremov M Y, Zhang M, Zhang Z, and Allen L H (2003) The design and operation of a MEMS differential scanning nanocalorimeter for high-speed heat capacity measurements of ultrathin films. *J. Microelectromechanical Syst.* 12(3): 355-364.

[49] Allard L F, Bigelow W C, Jose-Yacaman M, Nackashi D P, Damiano J, and Mick S E (2009) A new MEMS-based system for ultra-high-resolution imaging at elevated temperatures. *Microsc. Res. Tech.* 72: 208-215.

[50] Creemer J F, Helveg S, Kooyman P J, Molenbroek A M, Zandbergen H W, and Sarro P M (2010) A MEMS reactor for atomic-scale microscopy of nanomaterials under industrially relevant conditions. *J. Microelectromechanical Syst.* 19(2): 254-264.

[51] Hotovy I, Rehacek V, Mika F, Lalinsky T, Hascik S, Vanko G, and Drzik M (2008) Gallium arsenide suspeded microheater for MEMS sensor arrays. *Microsyst. Technol.* 14: 629-635.

[52] Mele L, Rossi T, Riccio M, Iervolino E, Santagata F, Irace A, Breglio G, Creemer J F, and Sarro P M (2011) Electro-thermal analysis of MEMS microhotplates for the optimization of temperature uniformity. *Procedia Eng.* 25: 387-390.

[53] Baroncini M, Placidi P, Cardinali G C, and Scorzoni A (2004) Thermal characterization of a mciroheater for micromachined gas sensors. *Sens. Actuator A Phys.* 115: 8-14.

[54] Zhao J, Liang L, Tang S, Zhang G, Su Y, Zhao Y, Li M, Zhang L, Fan S, Li Q, and Wei Y (2023) Graphene microheater chips for in situ TEM. *Nano Lett.* 23: 726-734.

[55] Bernal R A, Ramachandramoorthy R, and Espinosa H D (2015) Double-tilt in situ TEM holder with multiple electrical contacts and its application in MEMS-based mechanical testing of nanomaterials. *Ultramicroscopy.* 156: 23-28.

[56] Lee K, Park J, Jung S I, Hajra S, and Kim H J (2021) Direct integration of carbon nanotubes on a suspended Pt microheater for hydrogen gas sensing. *J. Mater. Sci. Materl. Electron.* 32: 19626-19634.

[57] Protochips, "Electrical E-chips - Finger Configuration - Fusion Select," [Online]. Available: https://protochips.shop/products/fusion-electrical-echips-finger. [Accessed 12 May 2023].

[58] Protochips, "Heating E-chips - Fusion Select," [Online]. Available: https://protochips.shop/products/fusion-thermal-echips. [Accessed 12 May 2023].

[59] Castagna M E, Modica R, Cascino S, Moschetti M, Cerantonio V, Messina A, and Santangelo A (2018) A high stability and uniformity W micro hot plate. *Sens. Actuator A Phys.* 279: 617-623.

[60] Diallo T M, Aziziyan M R, Arvinte R, Harmand J-C, Patriarche G, Renard C, Fafard S, Ares R, and Boucherif A (2022) In-situ transmission electron microscopy observation of germanium growth on freestanding graphene: unfolding mechanism of 3D crystal growth during van der waals epitaxy. *Small.* 18: 2101890.

[61] Protochips, "Technical Note: Closed Loop Temperature Control," [Online]. Available: https://www.protochips.com/wp-content/uploads/2017/11/tech-closed-loop-temperature-control.pdf. [Accessed 12 May 2023].

[62] DENSsolutions, "The revolutionary Wildfire Nano-Chip," [Online]. Available: https://denssolutions.com/products/wildfire/nano-chip/. [Accessed 12 May 2023].

[63] DENSsolutions, "Lightning In Situ TEM Biasing & Heating," [Online]. Available: https://denssolutions.com/products/lightning/. [Accessed 12 May 2023].

[64] Khanna V K, Prasad M, Dwivedi V K, Shekhar C, Pankaj A C, and Basu J (2007) Design and electro-thermal simulation of a polysilicon microheater on a suspended membrane for use in gas sensing. *Indian J. Pure Appl. Phys.* 45: 332-335.

930 [65] Laconte J, Dupont C, Flandre D, and Raskin J P (2004) SOI CMOS compatible low-
931 power microheater optimization for the fabrication of smart gas sensors. *IEEE Sens. J*4(5):
932 670-680.
933
934 [66] Sberveglieri G, Hellmich W, and Muller G (1997) Silicon hotplates for metal oxide gas
935 sensor elements. *Microsyst. Technol.* 3: 183-190.
936
937 [67] Rydberg M and Smith U (2000) Long-term stability and electrical properties of
938 compensation doped poly-Si IC-resistors. *IEEE Trans. Electron. Devices* 47(2): 417-426.
939
940 [68] El-Zoka A A, Howe J Y, Newman R C, and Perovic D D (2019) In situ STEM/SEM
941 study of the coarsening of nanoporous gold. *Acta Mater.* 182: 67-77.
942
943 [69] Li M, Qiu C, Dogel S, Chen P, Perovic D D, and Howe J Y (2022) Microstructure-
944 dependent thermal stability of super-tetragonal nanocomposite films through in situ
945 TEM/EELS study. *ACS Appl. Mater. Interfaces.* 14: 52316-52323.
946
947 [70] Krisper R, Lammer J, Pivak Y, Fisslthaler E, and Grogger W (2022) The performance of
948 EDXS at elevated sample temperatures using a MEMS-based in situ TEM heating system.
949 *Ultramicroscopy.* 234: 113461.
950
951 [71] Boyes E D and Gai P L (1997) Environmental high resolution electron microscopy and
952 applications to chemical science. *Ultramicroscopy*. 67: 219-232.
953

954 [72] Yokosawa T, Alan T, Pandraud G, Dam B, and Zandbergen H (2012) *In-situ* TEM on
955 (de)hydrogenation of Pd at 0.5–4.5 bar hydrogen pressure and 20-400 °C. *Ultramicroscopy* .
956 112(1): 47-52.
957
958 [73] Yaguchi T, Suzuki M, Watabe A, Nagakubo Y, Ueda K, and Kamino T (2011)
959 Development of a high temperature–atmospheric pressure environmental cell for high-
960 resolution TEM. *J Electron Microsc.* 60(3): 217-225.
961
962 [74] Hashimoto H*,* Naiki T*,* Watanabe M, Eto T, Fujiwara K and Nagahama Y (1966) Specimen
963 chamber for observing the reaction process with gas at high temperature. *Proc. 6th Int. Congr.*
964 *for Electron Microscopy.* Kyoto 1 :181.
965
966 [75] Hashimoto H, Naiki T, Mannami M and Fujita K (1959) Electron Microscopic Study by
967 Cine Film, *Structure and Property of Thin Film.* pp.71-86 (Neugebauer, Newkirk, Vermilyea.,
968 John Wiley & Sons Inc.).
969
970 [76] Baker RTK, Harris PS (1972) Controlled atmosphere electron microscopy. *J Phys E: Sci*
971 *Instrum*. 5(8): 793-797.
972
973 [77] Hashimoto H, Tanaka K, Yoda E (1958) A specimen treating device at high temperature
974 for the electron microscope. *J Electron Microsc.* 6(1): 8–11.
975
976 [78] FEI Company, "Titan ETEM G2," 2012. [Online]. Available:
977 https://photos.labwrench.com/equipmentManuals/14127-5457.pdf. [Accessed 12 May 2023].

[79] ThermoFischer Scientific, "Themis ETEM," 2020. [Online]. Available: https://assets.thermofisher.com/TFS-Assets/MSD/Datasheets/themis-etem-datasheet.pdf. [Accessed 12 May 2023].

[80] Boyes E D, Ward M R, Lari L, and Gai P L (2013) ESTEM imaging of single atoms under controlled temperature and gas environment conditons in catalyst reaction studies. *Ann. Phys.* 525(6): 423-429.

[81] Kishita K, Sakai H, Tanaka H, Saka H, Kuroda K, Sakamoto M, Watabe A and Kamino T (2009) Development of an analytical environmental TEM system and its application. *J Electron Microsc.* 58(6): 331-339.

[82] Matsumoto H, Konno M, Sato T, Nagaoki I, Yaguchi T and Howe J (2013) Simultanious *in situ* SEM and STEM analysis of gas/catalyst reaction in a cold field-emission environmental TEM. *Microscopy and Analysis.* 27(7): 13-18.

[83] Shirai M, Hanawa A, Kikuchi H, Inada H, Matsumoto H (2019) In-situ observation of catalytic reaction in gas atmosphere using an aberration corrected STEM. *Microsc Microanal*. 25(S2):1526-1527.

[84] Lv H, Lin L, Zhang X, Li R, Song Y, Matsumoto H, Ta N, Zeng C, Fu Q, Wang G, and Bao X (2021) Promoting exsolution of RuFe alloy nanoparticles on $Sr_2Fe_{1.4}Ru_{0.1}Mo_{0.5}O_{6-\delta}$ via repeated redox manipulations for CO_2 electrolysis. *Nature Communications*.12: 5665.

[85] Kamino T, Yaguchi T, Konno M, Watabe A, Marukawa T, Mima T, Kuroda K, Saka H, Arai S, Makino H, Suzuki Y and Kishita K.(2005) Development of a gas injection/specimen heating holder for use with transmission electron microscope. *J Electron Microsc.* 54(6): 497−503.

[86] Yaguchi T, Kanemura T, Shimizu T, Imamura D, Watabe A and Kamino T (2012) Development of a technique for in situ high temperature TEM observation of catalysts in a highly moisturized air atmosphere, *J Electron Microsc.* 61(4): 199–206.

[87] Kamino T, Yaguchi T, Konno M, Watabe A and Nagakubo Y (2006) Development of a specimen heating holder with an evaporator and gas injector and its application for catalyst. *J Electron Microsc.* 55(5): 245–252.

[88] Tsukasaki H, Igarashi K, Wakui A, Yaguchi T, Nakajima H, Kimura T, Sakuda A, Tatsumisago M, Hayashi A and Mori S (2021) *In situ* observation of the deterioration process of sulfide-based solid electrolytes using airtight and air-flow TEM systems. *Microscopy*. 24: 519-525.

[89] Tao F F and Crozier P A (2016) Atomic-scale observations of catalyst structures under reaction conditions and during catalysis. *Chem. Rev.* 116: 3487-3539.

[90] Gai P L, Boyes E D, Helveg S, Hansen P L, Giorgio S, and Henry C R (2007) Atomic-resolution environmental transmission electron microscopy for probing gas-solid reactions in heterogeneous catalysis. *MRS Bull.* 32: 1044-1050.

[91] Crewe A V, Wall J, and Langmore J (1970) Visibility of single atoms. *Science.* 168(3937): 1338-1340.

[92] Boyes E D, LaGrow A P, Ward M R, Martin T E, and Gai P L (2020) Visulizing single atom dynamics in heterogeneous catalysis using analytical in situ environmental scanning transmission electron microscopy. *Philos. Trans. Royal Soc. A* 378(20190605): 1-23.

[93] Martin T E, Mitchell R W, Boyes E D, and Gai P L (2020) Atom-by-atom analysis of sintering dynamics and stability of Pt nanoparticle catalysts in chemical reactions. *Philos. Trans. Royal Soc. A* 378(20190597): 1-21.

[94] Yuan W, Zhu B, Fang K, Li X Y, Hansen T W, Ou Y, Yang H, Wagner J B, Gao Y, Wang Y, and Zhang Z (2021) In situ manipulation of the active Au-TiO_2 interface with atomic precision during CO oxidation. *Science.* 371: 517-521.

[95] Yuan W, Fang K, You R, Zhang Z, and Wang Y (2023) Toward in situ atomistic design of catalytic active sites via controlled atmosphere transmission electron microscopy. *Acc. Mater. Res.* 4: 275-286.

[96] Ito T and Hiziya K (1958) A Specimen Reaction Device for the Electron Microscope and its Applications. *Journal of Electron Microscopy.* 6: 4-8.

[97] Hashimoto A, Han Y, Akimoto H, Hozumi R and Takeguchi M (2021) Development of a gas environmental heating specimen holder system using differential pumping. *Microscopy.*

70: 545-549.

[98] Shoji S, Peng X, Imai T, Kumar P S M, Higuchi K, Yamamoto Y, Tokunaga T, Arai S, Ueda S, Hashimoto A, Tsubaki N, Miyauchi M, Fujita T, and Abe H (2019) Topologically immobilized catalysis centre for long-term stable carbon dioxide reforming of methane. *Chemical Science.* 10: 3701-3705.

[99] Tanaka N, Usukura J, Kusunoki M, Saito Y, Sasaki K, Tanji T, Muto S, and Arai S (2013) Development of an environmental high-voltage electron microscope for reaction science. *Microscopy.* 62: 205-215.

[100] Tanaka N, Fujita T, Takahashi Y, Yamasaki J, Murata K, and Arai S (2020) Progress in environmental high-voltage transmission electron microscopy for nanomaterials. *Phil. Trans. R. Soc. A*. 378: 20190602.

[101] Muto S, Arai S, Higuchi S, Orita K, Ohta S, Tanaka H, Suganuma T, Ibe M, and Hirata H (2019) Environmental high-voltage S/TEM combined with quadrupole mass spectrometer for concurrent in-situ structural characterization and detection of product gas molecules associated with chemical reactions. *Microscopy.* 68: 185-188.

[102] Fujita T, Higuchi K, Yamamoto Y, Tokunaga T, Arai S, and Abe H (2017) In-Situ TEM Study of a Nanoporous Ni–Co Catalyst Used for the Dry Reforming of Methane. *Metals.* 7(10): 406.

[103] Alan T, Yokosawa T, Gaspar J, Pandraud G, Paul O, Creemer F, Sarro P M, and Zandbergen H W (2012) Micro-fabricated channel with ultra-thin yet ultra-strong windows enables electron microscopy under 4-bar pressure. *Appl. Phys. Lett. 1*00:081903.

[104] Protochips Inc., "Atmosphere AX: Machine Vision Environmental Cell for TEM," [Online]. Available: https://www.protochips.com/products/atmosphere/. [Accessed 10 June 2023].

[105] Dai S, Zhang S, Katz M B, Graham G W, and Pan X (2017) In situ observation of Rh-$CaTiO_3$ catalysts during reduction and oxidation treatments by transmission electron microscopy. *ACS Catal.* 7(3): 1579-1582.

[106] Ross F M (2016) Liquid Cell Electron Microscopy.In Ross F M(ed.) *Advances in Microscopy and Microanalysis* (Cambridge University Press, Cambridge).

[107] DiCecco LA, Gao R, Athanasiadou D, Chan RL, Carneiro KMM, Kelly DF, Sone E, Grandfield K(2022) Exploring Calcium Phosphate Biomineralization Systems Using In Situ Liquid Phase Electron Microscopy *Microsc Microanal.* 28(S1):1818-1820.

[108] Abrams I M and McBain J W (1944) A closed cell for electron microscopy. *Science.* 100(2595): 273-274.

[109] Williamson M J, Tromp R M, Vereecken P M, Hull R, and Ross F M (2003) Dynamic microscopy of nanoscale cluster growth at the solid-liquid interface. *Nat. Mater.* 2(8): 532-536.

[110] Zheng H, Smith R K, Jun Y W, Kisielowski C, Dahmen U, and Alivisatos A P (2009) Observation of single colloidal platinum nanocrystal growth trajectories. *Science.* 324(5932): 1309-1312.

[111] Hummingbird Scientific, "Optical Bulk Liquid Electrochemistry," [Online]. Available: https://hummingbirdscientific.com/products/optical-bulk-liquid/. [Accessed 16 May 2023].

[112] Prozorov T, Almeida T P, Kovacs A, and Dunin-Borkowski R E (2017) Off-axis electron holography of bacterial cells and magnetic nanoparticles in liquid. *J. R. Soc. Interface.* 14(20170464): 1-10.

[113] Yuk J M, Park J, Ercius P, Kim K, Hellebusch D J, Crommie M F, Lee J Y, Zettl A, and Alivisatos A P (2012) High-Resolution EM of Colloidal Nanocrystal Growth Using Graphene Liquid Cells. *Science*. 336(6077): 61-64.

[114] Clark N, Kelly D J, Zhou M, Zou Y C, Myung C W, Hopkinson D G, Schran C, Michaelides A, Gorbachev R, and Haigh S J (2022) Tracking single adatoms in liquid in a transmission electron microscope. *Nature.* 609(7929): 942-947.

[115] Kuwahara M, Agemura T (2023) Temporal resolution in transmission electron microscopy using a photoemission electron source. *Microscopy,* 72(2):97-110.

[116] Kim J S, Langrange T, Reed B W, Taheri M L, Armstrong, King W.E, Browning N D, Campbell G H (2008) Imaging of Transient Structures Using Nanosecond in Situ TEM. *Science* 321(5895):1472-1475.

Figure Legends

Figure 1 *In-situ* annealing system is constituted of a double tilt furnace type heating holder and thermal control box with a Proportional-Integral-Differential (PID) controller. Reproduced from reference [30], with the permission of Oxford University Press.

Figure 2 An external view of the direct type of side-entry single tilt heating holder, "Kamino holder". A fine W filament of 25 μm in diameter, which is bridged across two electrodes, is heated by direct electric current from a battery.

Figure 3 Schematic diagram of a holder consists of the 3 mm-diameter-grid having a support film and 2 W-filaments for sample evaporation. Reproduced from reference [37], with the permission of The Japanese Society of Microscopy.

Figure 4 Scanning Ion Microscope images showing a typical sample preparation sequence for the *in-situ* observation of the interface reaction. (a) The sampling area. (b) After the W-deposition. (c) After the sputtering of surrounding area. (d) After cutting of the bottom. (e) Picking out from the substrate. (f) Attaching to the filament. (g) The space between the sample and the filament, after filling with the W-deposition. (h) After thinning. Reproduced from reference [39], with the permission of Oxford University Press.

Figure 5. Double spiral heating element designs by (a) Perez Garza et al.[42], (b) Mele et al.[47], and (c) van Omme et al.[44]. (a) shows the heating element that follow an octagonal shape

using straight line segments; (b) shows the NanoEx™ -i/v microheater chip, which concentrates all the electron-transparent windows in a central large circle. Each window is SiN and consists of several through holes; (c) shows the Nano-Chip in the Wildfire heating holder. The heating element of the Nano-Chip has increasing linewidth towards the centre of the double spiral with no sharp corners and displays excellent temperature uniformity; All images are reproduced with permission from the respective references.

Figure 6 Schematic diagram of “opened type” specimen chamber(a) and “closed type” one(b).

Figure 7 External view of the gas injection/specimen heating holder. A gas injection nozzle with an inner diameter of 0.5 mm was built about 1mm away from the heating element. This holder provides localized gas atmosphere near the specimen.

Figure 8 Procedure for synthesis of metal oxide support and deposition of catalyst nano-particles in a TEM specimen chamber using the specimen heating holder equipped with a gas injection nozzle and an evaporator. (a) Oxidation of metal to synthesize metal oxide support. (b) Deposition of catalyst nano-particles on the metal oxide support. (c) Observation of the nano-catalyst at various environments.

Figure 9 External view of the tip of the TEM air protection transfer holder with a W filament and gas injection nozzle. (a) Shutter off, (b)Shutter on.

Figure 10 "Open-type" specimen holder with MEMS heating device. (a) Schematic diagram of the holder consisting of a differential pumping unit and a heating unit. (b) Interior of the specimen holder grip with a gas tank and piezo-driven fine control valve. Cross-sectional illustration (c) and photograph (d) of the specimen holder head with orifices, membrane-type heater, and pressure gage. Reproduced from reference [97], with the permission of Oxford University Press.

Figure 11 *In-situ* STEM observation on Ni#Y_2O_3. (a) EDX elemental mapping image of Ni#Y_2O_3 sliced specimen. Green: Y; Red: Ni. (b) *In situ* annular dark-field STEM image before the catalytic reaction (in vacuum at 450 ºC) and (c) during the CH_4 conversion condition (0.3 Pa CH_4+CO_2 gas at 450 ºC). Reproduced from reference [98], with the permission of Royal Society of Chemistry.

Figure 12 (a) Illustration of a general view of E-HVEM. Reproduced from reference [99], with the permission of Oxford University Press. (b) Cross-sectional illustrations of a side-entry goniometer to enable insertion of the gas chamber as an environmental cell from the left-hand side. Reproduced from reference [100], with the permission of the Royal Society Publishing.

Figure 13 Atomic-scale in situ gas study performed using E-cell. (a) and (b) Protochips

Atmospheric AX gas cell [104]. HAADF image of Rh-$CaTiO_3$ powder in 760 Torr of 5%H_2/Ar (labeled by R) after 12 min at 500 °C: (c) large field of view shows diffuse sub-nanometer bright regions and occasional bright spots, marked by yellow arrows; (d) enlarged image, containing the small rectangular box in panel (c), where Ca (blue) and Ti (magenta) columns are identified; and (e) intensity along a line scanned from left to right within the rectangular box in panel (d); Reproduced with permission from reference[105].

Figure 14 Configuration of the graphene-MoS2-hBN liquid cell. Reproduced with permission from reference [114].

Figure 1

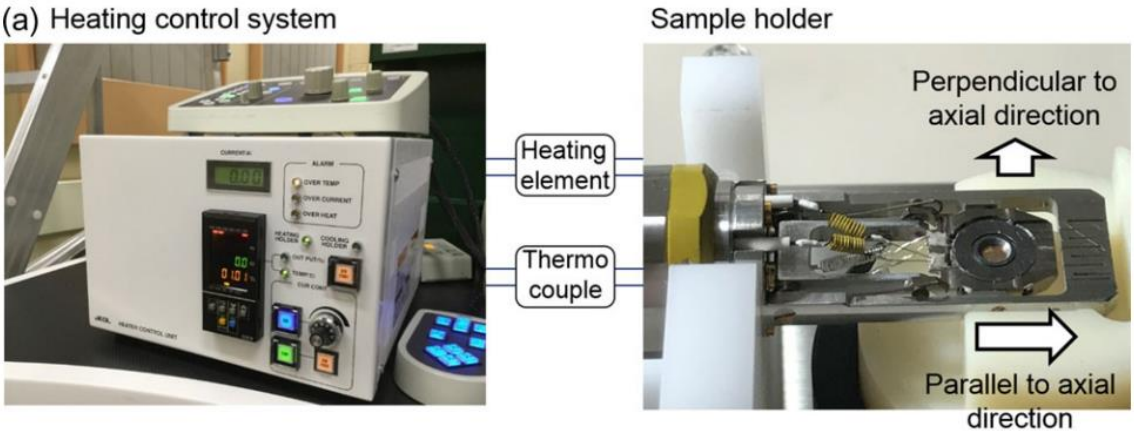
(a) Heating control system
Sample holder
Heating element
Thermo couple
Perpendicular to axial direction
Parallel to axial direction

Figure 2

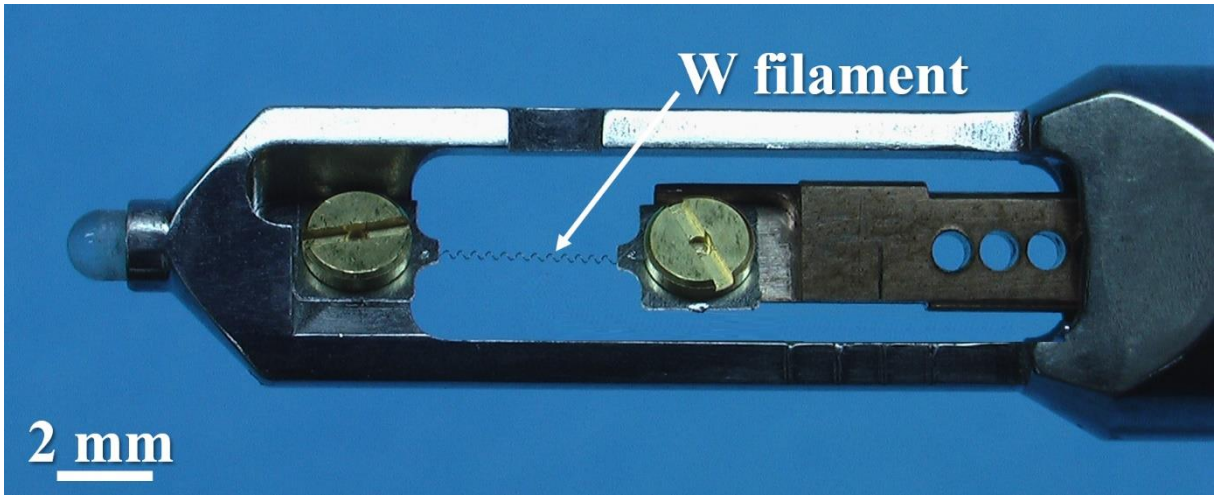

Figure 3

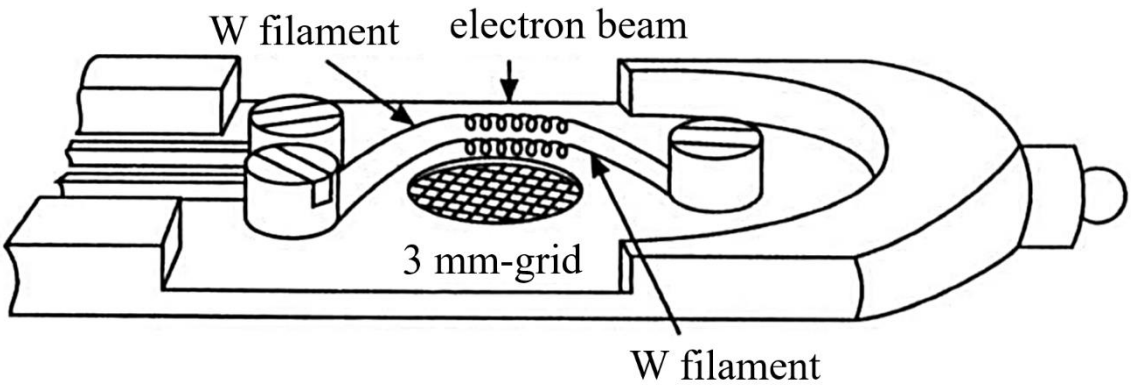

Figure 4

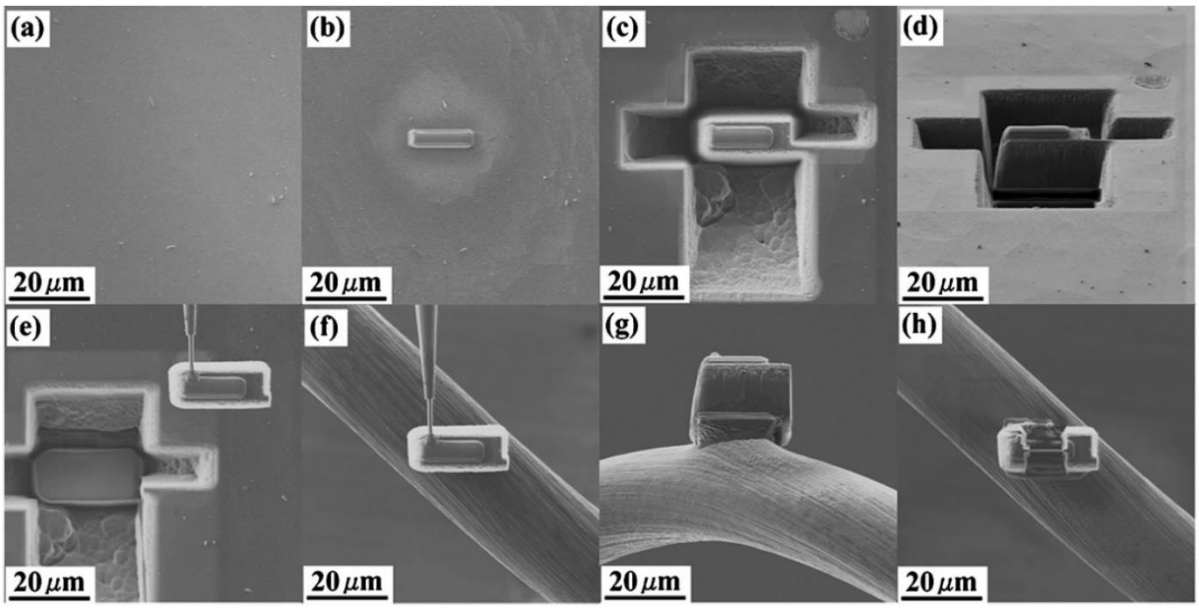

Figure 5

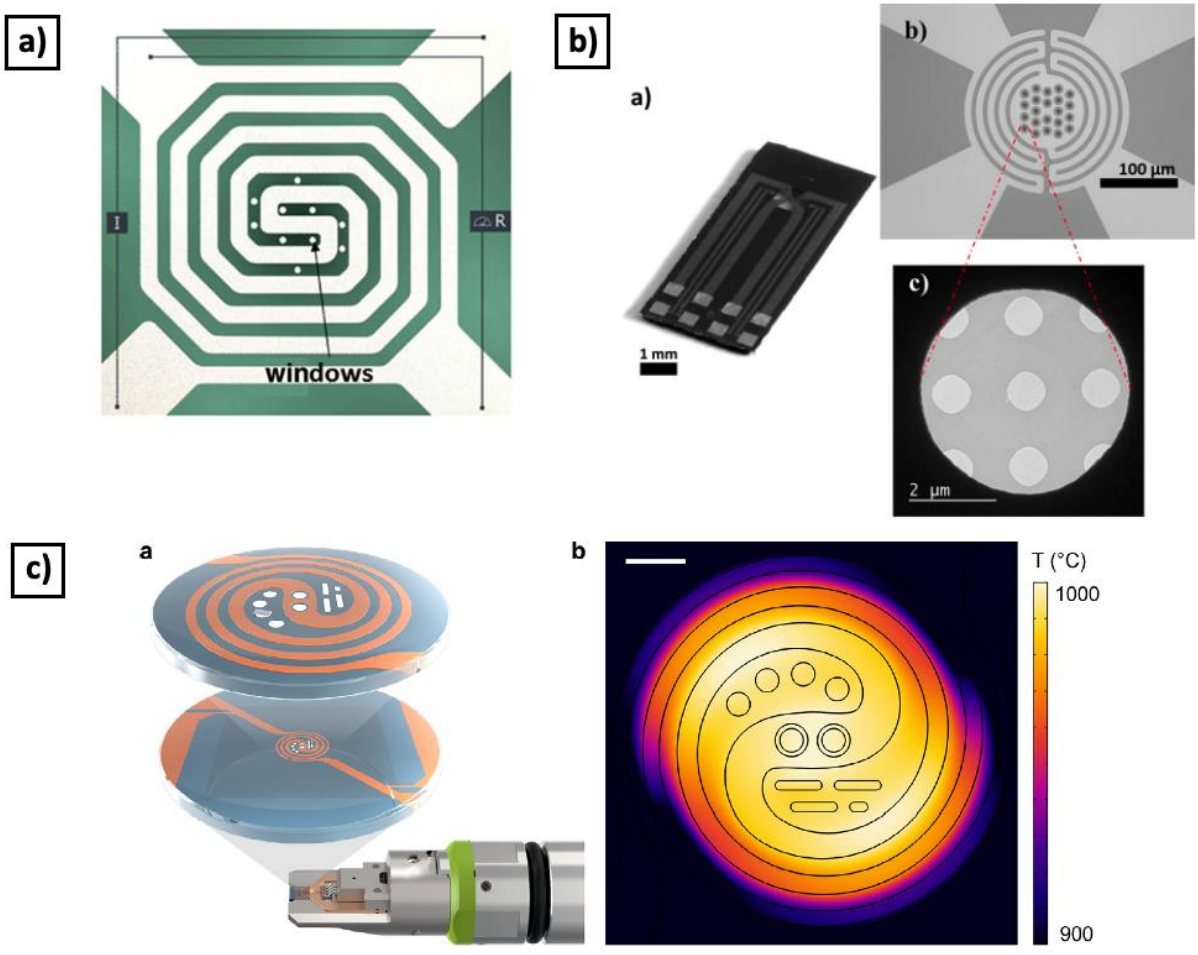

Figure 6

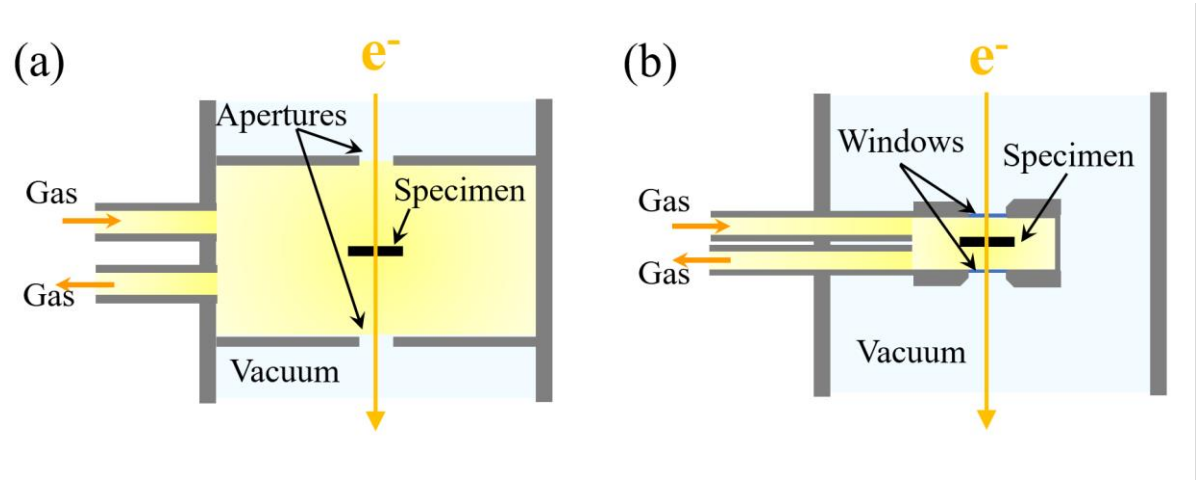
(a)
e⁻
Apertures
Gas
Specimen
Gas
Vacuum
(b)
e⁻
Windows
Specimen
Gas
Gas
Vacuum

Figure 7

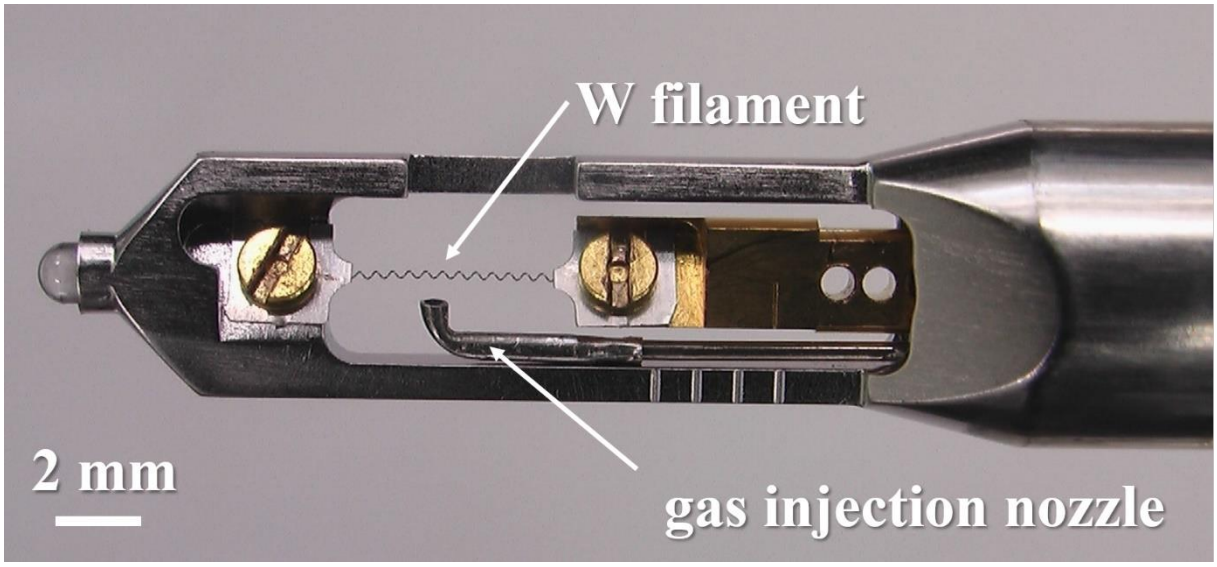

Figure 8

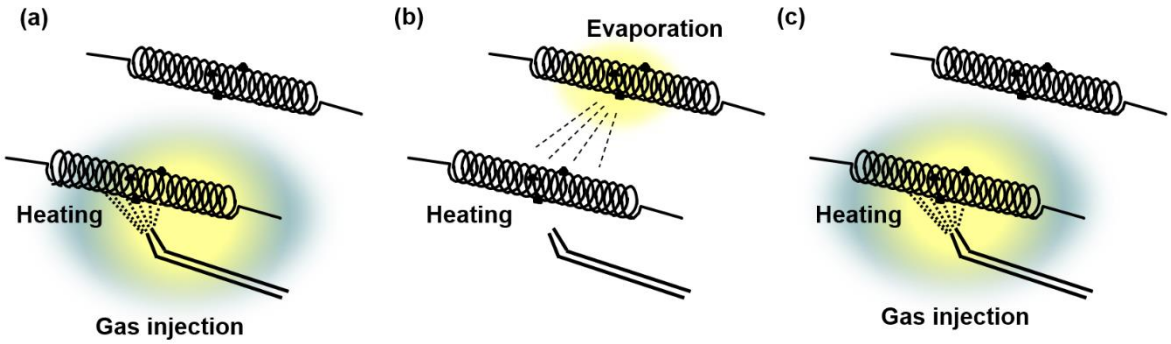
(a)
Heating
Gas injection
(b)
Evaporation
Heating
(c)
Heating
Gas injection

Figure 9

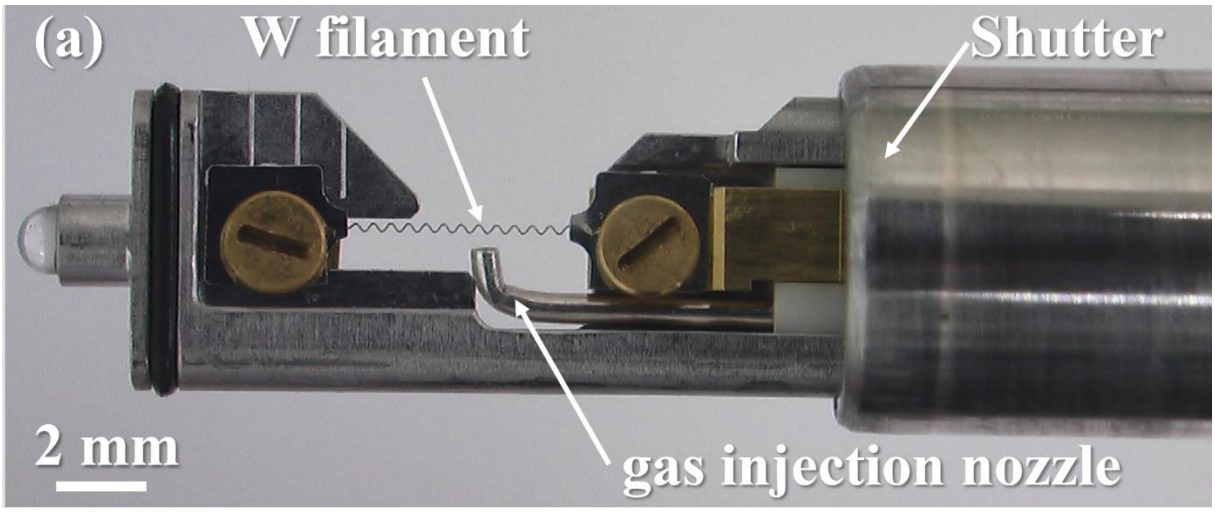

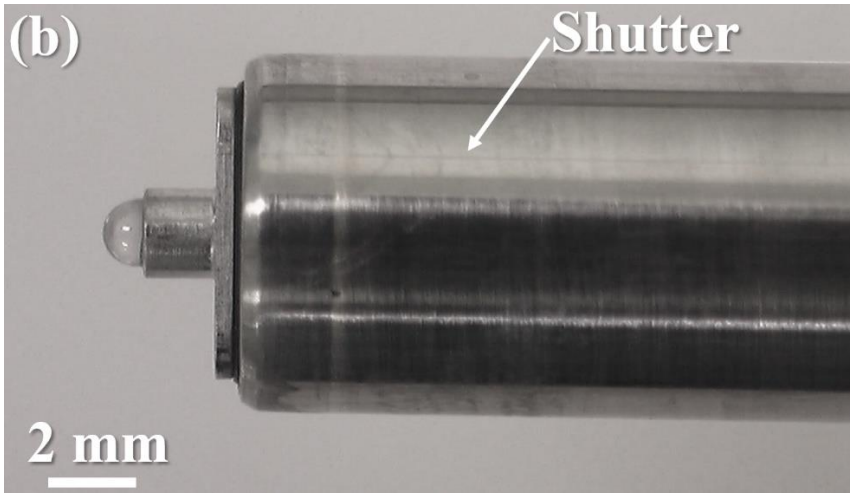

Figure 10

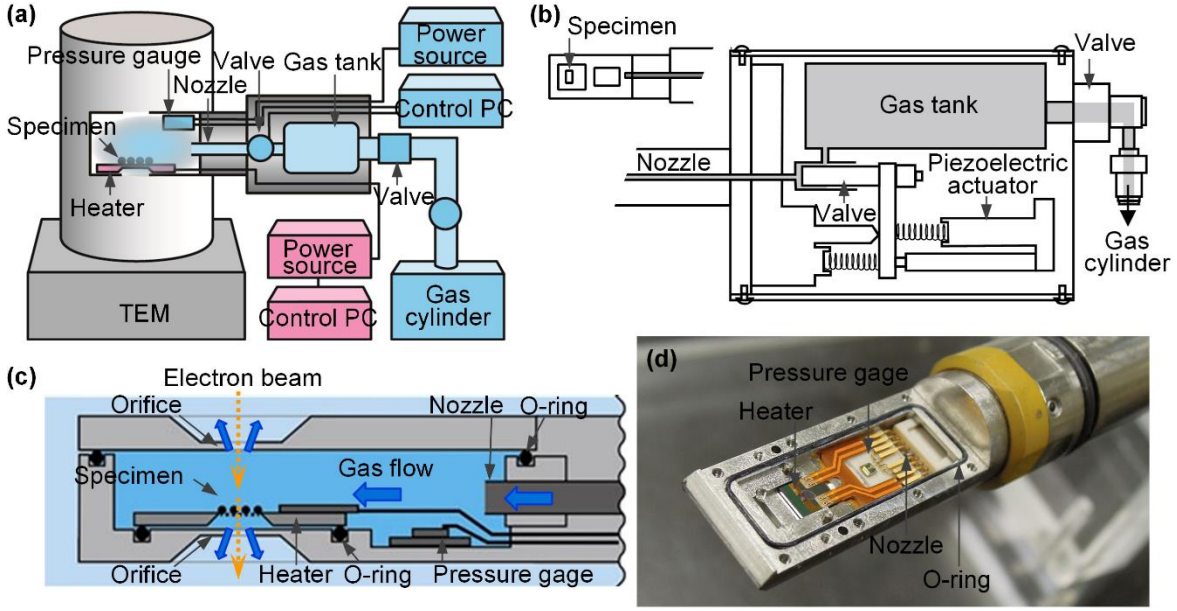
(a)
Pressure gauge
Nozzle
Valve
Gas tank
Power source
Control PC
Specimen
Heater
Valve
Power source
Control PC
Gas cylinder
TEM
(b)
Specimen
Valve
Gas tank
Nozzle
Piezoelectric actuator
Valve
Gas cylinder
(c)
Electron beam
Orifice
Nozzle
O-ring
Specimen
Gas flow
Orifice
Heater
O-ring
Pressure gage
(d)
Pressure gage
Heater
Nozzle
O-ring

Figure 11

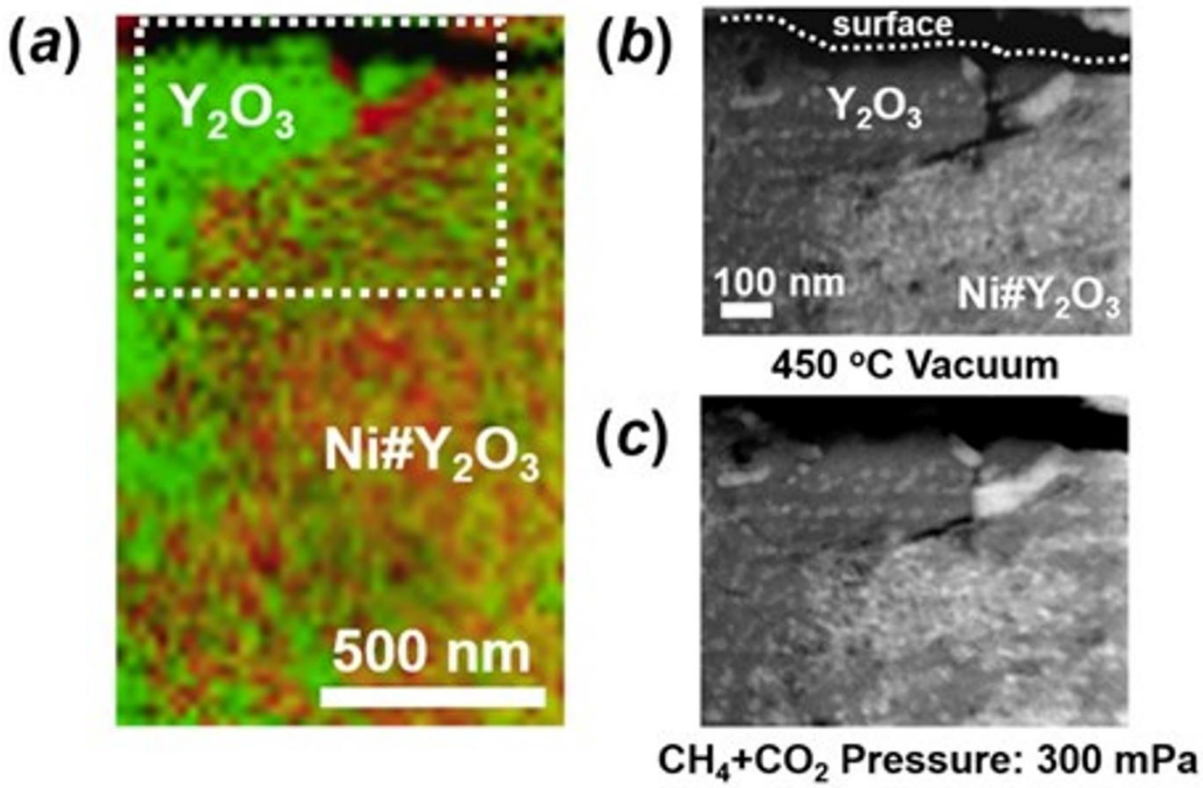
(a)
Y_2O_3
$Ni\#Y_2O_3$
500 nm
(b)
surface
Y_2O_3
100 nm
$Ni\#Y_2O_3$
450 °C Vacuum
(c)
CH_4+CO_2 Pressure: 300 mPa

Figure 12

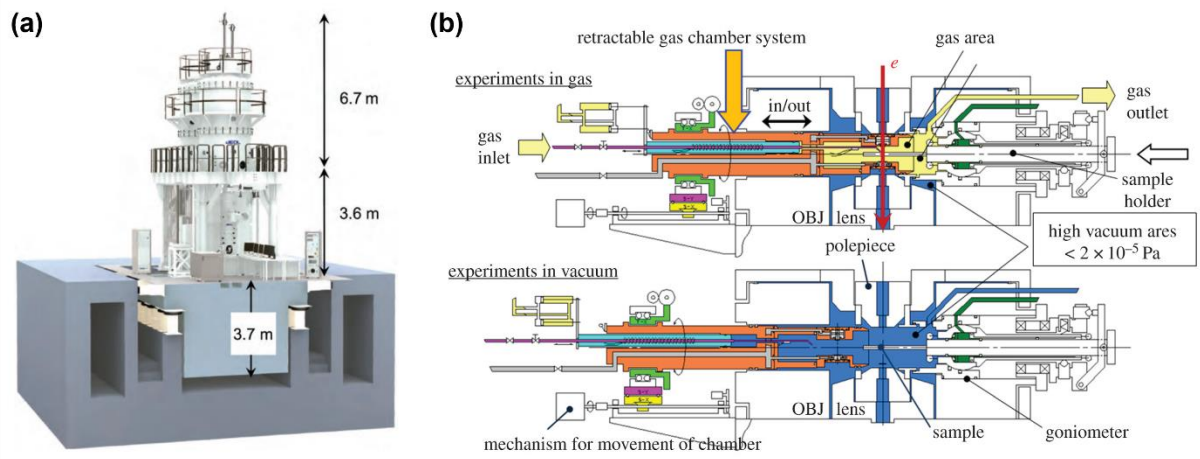
(a)
6.7 m
3.6 m
3.7 m
(b)
retractable gas chamber system
gas area
experiments in gas
e
in/out
gas
inlet
gas
outlet
sample
holder
OBJ lens
high vacuum ares
< 2 × 10⁻⁵ Pa
polepiece
experiments in vacuum
OBJ lens
sample
goniometer
mechanism for movement of chamber

Figure 13

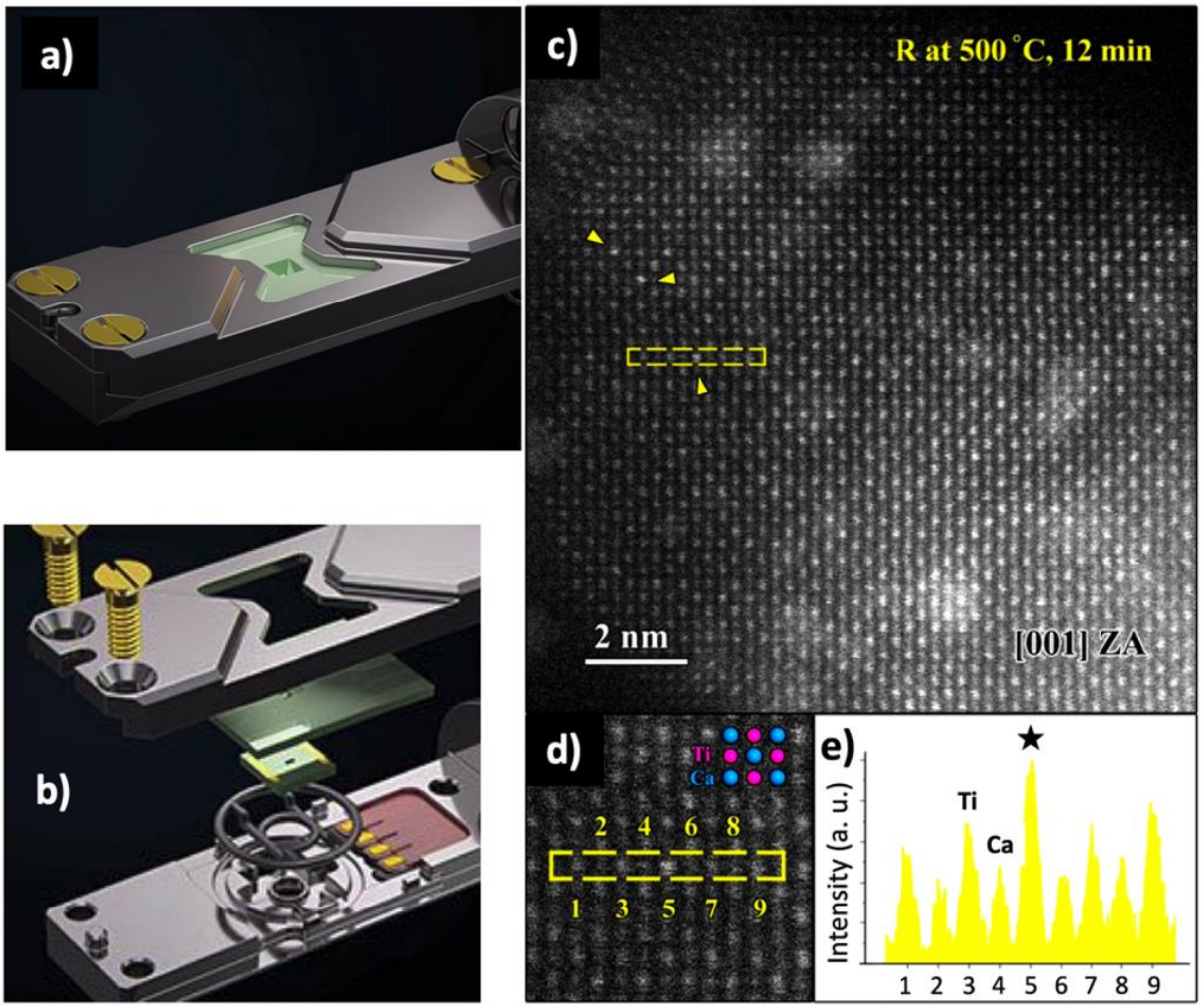
a)
b)
c)
R at 500 °C, 12 min
2 nm
[001] ZA
d)
Ti
Ca
2 4 6 8
1 3 5 7 9
e)
Intensity (a. u.)
Ti
Ca
1 2 3 4 5 6 7 8 9

Figure 14

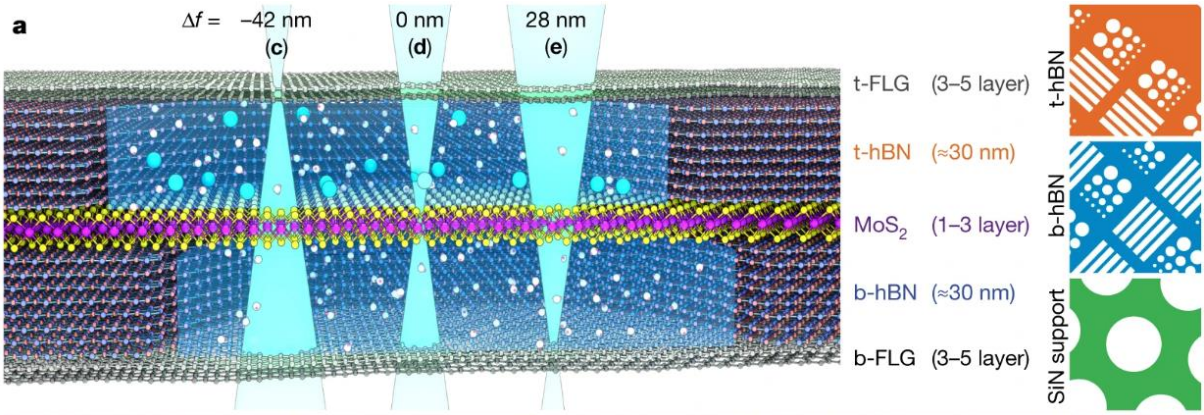
a
Δf = −42 nm
(c)
0 nm
(d)
28 nm
(e)
t-FLG (3–5 layer)
t-hBN (≈30 nm)
MoS2 (1–3 layer)
b-hBN (≈30 nm)
b-FLG (3–5 layer)
t-hBN
b-hBN
SiN support